(1)

ARMY RESEARCH LABORATORY

Effect of Variation of the Angle Between Joined Armor Plates on Ballistic Shock Attenuation

Ricky L. Grote

ARL-TR-466 June 1994

NOTICES

Destroy this report when it is no longer needed. DO NOT return it to the originator.

Additional copies of this report may be obtained from the National Technical Information Service, U.S. Department of Commerce, 5285 Port Royal Road, Springfield, VA 22161.

The findings of this report are not to be construed as an official Department of the Army position, unless so designated by other authorized documents.

The use of trade names or manufacturers' names in this report does not constitute indorsement of any commercial product.

REPORT DOCUMENTATION PAGE

Form Approved
OMB No. 0704-0188

1. AGENCY USE ONLY (Leave blank)	2. REPORT DATE	3. REPORT TYPE AND DATES COVERED
	June 1994	Final, Jan 93–Nov 93

4. TITLE AND SUBTITLE

Effect of Variation of the Angle Between Joined Armor Plates on Ballistic Shock Attenuation

5. FUNDING NUMBERS

4F592-Y62-63-U600

6. AUTHOR(S)

Ricky L. Grote

7. PERFORMING ORGANIZATION NAME(S) AND ADDRESS(ES)

U.S. Army Research Laboratory
ATTN: AMSRL-SL-BS
Aberdeen Proving Ground, MD 21005-5066

8. PERFORMING ORGANIZATION REPORT NUMBER

9. SPONSORING/MONITORING AGENCY NAME(S) AND ADDRESS(ES)

U.S. Army Research Laboratory
ATTN: AMSRL-OP-AP-L
Aberdeen Proving Ground, MD 21005-5066

10. SPONSORING/MONITORING AGENCY REPORT NUMBER

ARL-TR-466

11. SUPPLEMENTARY NOTES

12a. DISTRIBUTION/AVAILABILITY STATEMENT

Approved for public release; distribution is unlimited.

12b. DISTRIBUTION CODE

13. ABSTRACT (Maximum 200 words)

Ballistic shock has been recognized by the vulnerability community as a damage-producing mechanism worthy of investigation. A simple straight line analysis method has been proposed and is being pursued. One factor not considered to this point is the effect of angle variation between welded plates on shock attenuation. The object of this research effort was to determine if such an effect exists, and, if so, a determination of the effect was desired.

Both experimental and computational analyses were conducted in an attempt to investigate the effect of angle variation on shock attenuation. Mild steel and 5083 aluminum target plates were constructed. The angle variation in the target plates ranged from 0° to 120°, 0° being a flat plate. A steel ball bearing was used as an impacting device, and accelerometers were used to obtain the desired experimental data. ADINA was used for the computational portion of this effort, and all experimental conditions were analyzed via this code.

As a result of this effort, it was shown that angle variation does have an effect on shock attenuation, and algorithms were developed that quantify the effect. Work in this area of interest must continue to further investigate these effects on other plate materials and different welding techniques. Additional effort could also be placed on analyzing these effects with differing impactor types.

14. SUBJECT TERMS	15. NUMBER OF PAGES
ballistic shock, attenuation, armor, welded plates, aluminum, mild steel, acceleration	68
	16. PRICE CODE

17. SECURITY CLASSIFICATION OF REPORT	18. SECURITY CLASSIFICATION OF THIS PAGE	19. SECURITY CLASSIFICATION OF ABSTRACT	20. LIMITATION OF ABSTRACT
UNCLASSIFIED	UNCLASSIFIED	UNCLASSIFIED	UL

INTENTIONALLY LEFT BLANK.

ACKNOWLEDGMENTS

It is necessary to acknowledge several individuals without whom this effort would not have been possible. Dr. Jack Vinson is acknowledged for the guidance he provided throughout this effort. Mr. John Jacobson receives my appreciation for providing the opportunity to further my education. Dr. Barry Bodt provided consultative services regarding data analysis and experimental design. Dr. Joseph Santiago and Mr. Fred Gregory provided access to the ADINA code and were available for comments on the finite element work. Mr. Ted Robinson is owed my sincerest gratitude for setting up the data acquisition system and for taking part in the conduct of the experimental program.

INTENTIONALLY LEFT BLANK.

TABLE OF CONTENTS

INTENTIONALLY LEFT BLANK.

LIST OF FIGURES

LIST OF TABLES

1. INTRODUCTION

Ballistic shock has been recognized as a damage mechanism capable of causing component failures in armored combat vehicles. Unfortunately, the vulnerability community has not been able to incorporate this phenomenon in its predictive models. Historically, the main penetrator and spall have been considered as the primary damage mechanisms; recently, however, ballistic shock has gained some attention as a lethal mechanism, and the U.S. Army now has a shock protection requirement for armored combat vehicles (Walton 1989). Thus, the incorporation of shock effects into vulnerability models has become a priority.

One method of incorporating the effects of ballistic shock into vulnerability codes could be to construct detailed finite element models of every armored combat vehicle and then somehow transfer the results to the vulnerability models. This, however, is an impractical approach, and a lower resolution method has been suggested by Walbert (1991). The fundamental concept behind Walbert's approach is to analyze a small set of simplified structures that could be used to represent classes of combat vehicles in an attempt to develop rules of thumb for shock attenuation. These rules of thumb could then be compared to experimental data, and as confidence is gained, detail could be added. Another simplification would be to analyze shock attenuation and propagation along the shortest straight path through a vehicle structure from point of impact to a response point of interest. A straight line analysis, for determining shock attenuation, has actually been used by Barrett (1975) for developing shock requirements for Viking Lander components. An important point to note is that both Walbert and Barrett were aware of the need to analyze shock effects at the component level of a system instead of attempting to make a bigger leap to some sort of loss of system capability or utility. This is important because analyzing to the component level will allow the results of a shock analysis to be incorporated into vulnerability analyses at the same point as analyses performed for other damage-producing mechanisms. The point at which shock modeling would be incorporated into the vulnerability process is termed the $O_{1,2}$ mapping (Klopcic, Starks, and Walbert 1992). There are four spaces within the vulnerability process as described by Deitz et al. (1990). These spaces of vulnerability are (1) weapon/target initial conditions, (2) the set of damaged components, (3) measures of system performance, and (4) measures of system effectiveness. The $O_{1,2}$ mapping is the method by which one gets from a weapon/target interaction to a set of damaged components. In this case, the desired mapping is an algorithm that translates the interaction to ballistic shock damage potential for components.

If, in fact, one wishes to incorporate ballistic shock effects in the vulnerability process, using the straight line approach mentioned previously, then an additional parameter that must be considered is the attenuation of shock due to welded joints between armor plates positioned at various angles. The effect of angle variation between welded armor plates on shock or, in this case, acceleration attenuation is the primary subject of this research effort.

2. OBJECTIVES

It was the objective of this research effort to answer the following questions:

(1) Is there an effect on shock attenuation due to angle variation between welded plates?

(2) If the answer to the question above is yes, then what is the relationship between attenuation and the angle at which the plates are connected?

(3) Is the effect on attenuation due to angle variation constant over a range of plate materials and impact conditions?

(4) Can simple finite element modeling be used to determine attenuation factors for various plate configurations?

3. APPROACH

In order to meet the stated objectives, it was decided that both experimental and computational analyses would have to be conducted for an identical set of impact and target configurations. The analyses started with a flat plate to obtain baseline acceleration levels and then proceeded to angled plates to determine attenuation due to the geometry changes. The flat plate used for determining the baseline acceleration levels was actually two plates welded together. This was done in an attempt to filter out the effects the weld material would have on the attenuation. Target material and thickness were representative of actual armor used in military applications. The impact condition were such that they could be incorporated into a finite element model with a high level of confidence that they accurately depicted experimental impact conditions. Additionally, it was decided that the impact conditions would remain in the elastic range only. This was done to reduce the number of plates required for experimentation since

plates with permanent deformation could not be used for more than one experiment. Once both analyses were completed, the desired relationship between attenuation and angle was obtained, and the experimental results were compared to the computations to determine the applicability of the finite element modeling.

4. EXPERIMENTAL DESIGN

There were two issues concerning the experimental design that required consideration. These issues included the following:

(1) The experimental test matrix would have to allow for sufficient test replications and variations of parameters to ensure a good experimental design.

(2) The experimental setup would have to allow for appropriate data measurement and collection for a variety of test conditions.

4.1 Test Matrix. The first task was to determine the test parameters and their variations. Material type, plate angles, material thickness, and impact conditions were the parameters initially chosen for variation. The materials chosen were mild steel and 5083 aluminum. These materials were chosen because of their availability and the fact that they are commonly used in the design of armored combat vehicles. Initially, three material thicknesses (12.7 mm, 19 mm, and 38 mm) were selected because they represented actual armor thicknesses on some current vehicles. Due to quality control problems during the welding process and resource availability for refabrication of plates, only the 12.7-mm plates were used for this effort. It was decided that the impact conditions should be varied in the level of the impact force while using the same impacting device. This would allow the research to investigate the consistency of the acceleration attenuation without getting into other issues such as differing impactor characteristics. Finally, the parameter of main interest to this study—angle—was to be varied five times from 0° to 120° by 30° increments. It was felt that this gave a good range of angles and was also representative of typical armored vehicle geometries. Thus, the matrix ended up with 2 materials, 1 thickness, 3 impact levels, 5 angles, and 5 replications of each test condition for a total of 150 planned experiments. Figure 1 shows how the plate angles were measured for this exercise.

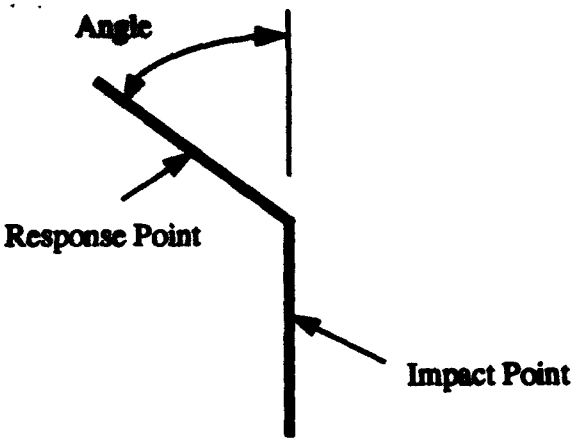

Figure 1. Measurement of plate angles.

4.2 Experimental Setup.

4.2.1 Target Plates. The design of the target plates was an important issue that had to be resolved early in this effort. The target plate geometry was needed for the computational work and impacted greatly on the experimental setup. It was decided that the flat plates would be twice as long as they were wide with dimensions of 30.5 cm × 61 cm (1 ft × 2 ft). The remaining plates were fabricated such that the outer dimensions of each half of the plates were 30.5 cm × 30.5 cm (1 ft square). Thus, the straight line distance, on the surface of the plate, from the impact location to the response point remained constant for all plates. This was accomplished by filling in the weld area with excess weld material and then grinding the weld material down until a straight sharp-edged corner was formed at the connection between the two pieces of plate material. Figure 2 is a photo of an actual target plate showing the sharp edge of an angle connection.

The 30.5-cm × 61-cm (1 ft × 2 ft) overall dimensions were chosen to allow for measurement of acceleration levels, at the response point, for several microseconds before reflections from the plate boundaries reached the response point. Thus, the experiments would capture the effect of the geometry at the welded joint on shock attenuation without interference from edge reflections or boundary conditions. Also, since the distance between the impact point and the response point was held constant, distance attenuation effects were eliminated. Table 1 presents material property data for the plates.

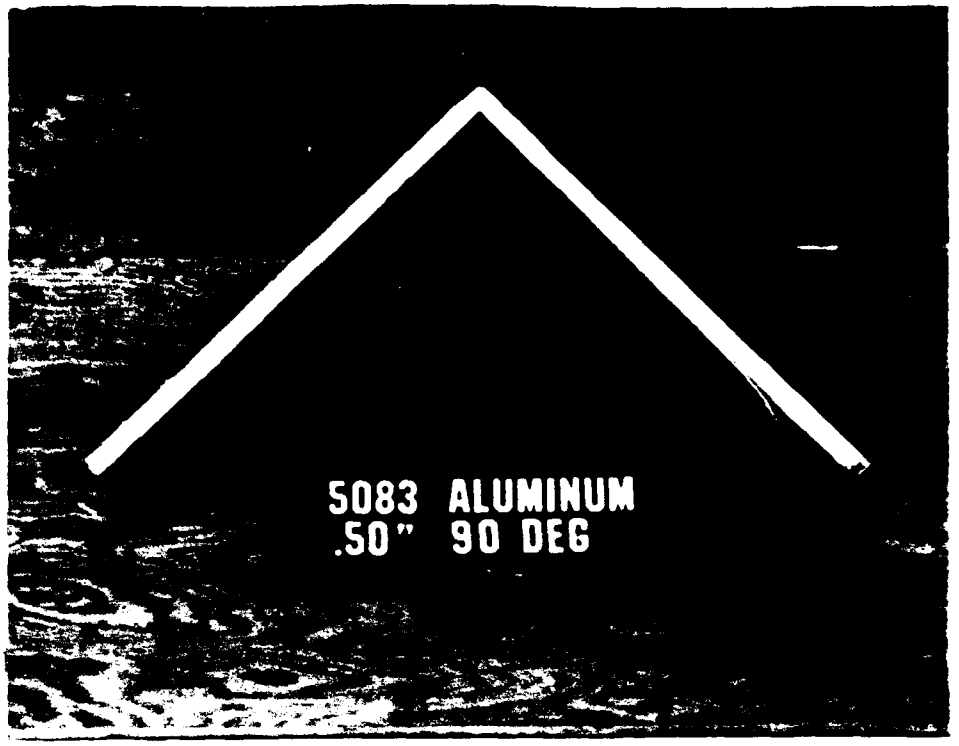

Figure 2. Example of a target plate.

Welding rods consisting of 5356 aluminum and carbon steel (tensile strength of 640 MPa) were used for joining the aluminum and mild steel plates, respectively.

Table 1. Target Plate Material Properties

Material	Modulus of Elasticity, E	Density, ρ (g/cm^3)	Poisson's Ratio, ν
Mild Steel	209 GPa	7.84	0.30
5083 AL	68950 MPa	2.66	0.336

Once fabricated, the target plates had to be prepared for experimentation. The center of each half of the plates was located and marked. The points directly behind these center points, on the opposite side of the plates, were also marked. One of the marked points on the front side of the plates was to be the impact point while the other three locations were to be used for instrumentation. These three locations were drilled and tapped, using a No. 21 drill bit and a 10–32 tap, to allow for mounting accelerometers.

The surfaces of the plates around these locations were sanded smooth to allow for flush mounting of the accelerometers. Figure 3 shows the location of the impact and response points on a plate.

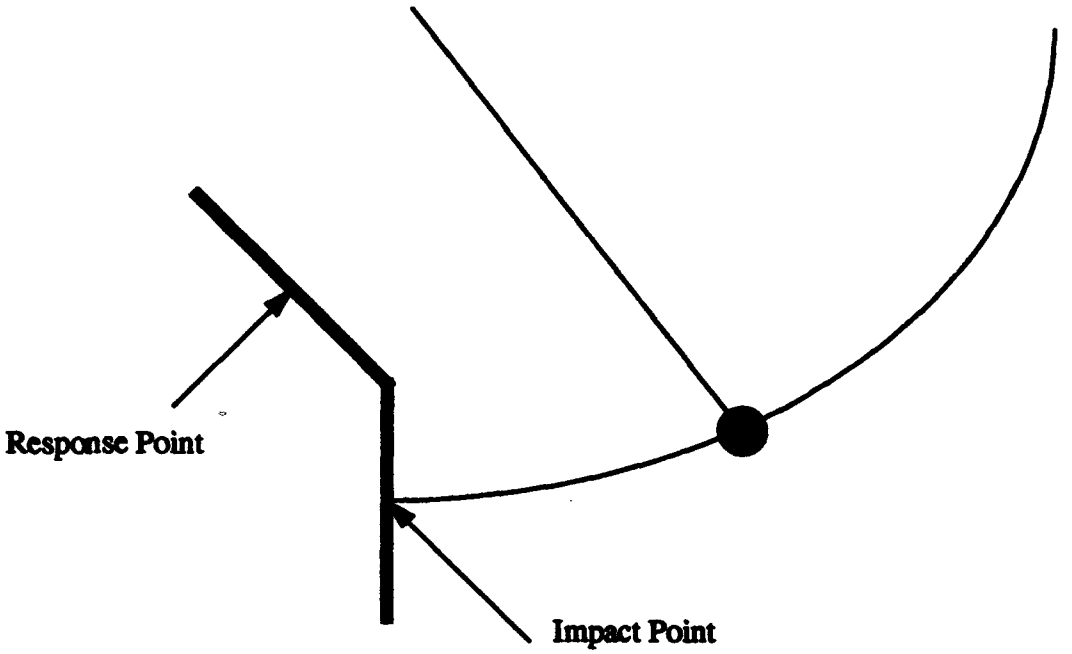

Figure 3. Impact and response point locations.

4.2.2 Test Stand. The mounting hardware for the target plates was an integral part of the experimental setup. A test stand which was capable of holding any of the target plates was designed and fabricated for this effort. It was imperative that the test stand be capable of mounting each of the different plates so as to eliminate any effects that different test fixtures could have on the experimental results. This test stand contained three major plates. The base of the fixture was a mild steel plate measuring 56 cm × 81 cm × 5 cm (22 in × 32 in × 2 in) thick. The other two main plates, also made of mild steel, were welded to the base plate in an upright position. These two plates measured 61 cm × 71 cm × 2.54 cm (24 in × 28 in × 1 in) thick. Both plates had 30.5 cm (1 ft) radial slots cut in them to allow for mounting hardware adjustments for fastening the different angled plates.

In addition to mounting the target plates, the test stand was also used to support the impacting mechanism. A two-wire pendulum, with a 2.54-cm-diameter steel ball bearing (70.74 g) attached to the end, was used as the impacting mechanism for this effort. The ball bearing was chosen to be the impactor primarily because a half-sine wave loading function has been shown to represent ball bearing impact conditions accurately (Walton 1985). The two-wire pendulum was chosen as the delivery mechanism because it would assure relatively consistent impact locations, was inexpensive, and was easily assembled.

Integration of the two-wire pendulum into the test fixture design was relatively simple. Two pieces of flat stock were attached to the top of the two side plates of the test stand such that they extend vertically above the fixture. Holes were then drilled in each piece of flat stock so that the pendulum wire could be threaded through and tied off. These holes were placed at 1 m above the proposed impact height on the target plates and were also positioned so that the pendulum would be at the bottom of its arc when the ball bearing would strike the target plate. Once threaded, the wires were adjusted until the ball bearing would impact at the center of the target plate at a height of 15 cm above the base of the test stand.

The final addition to the test stand was the release mechanism for the impacting device. It was recognized that consistent releases of the ball bearing, from accurately measured drop heights, were essential to the repeatability of the experiments. To accomplish both the consistent releases and the accurate determination of height, an adjustable protractor was mounted to the test fixture that allowed for accurate measurement of the angle of the pendulum and incorporated the use of an electromagnet as the release mechanism. Figure 4 is a photo of the test stand and impacting device.

4.3 Data Acquisition System. Data acquisition requirements for this effort included the measurement of the ball bearing rebound height after impact for calculating an approximate impact force and the measurement of acceleration as a function of time at the response point. The rebound height was approximated through the use of a video camera and a grid board. Three accelerometers were used for each experiment. The first accelerometer was always on the backside of the target plate directly behind the impact location. This accelerometer was a PCB Model 302A2, and it measured acceleration in a single axis normal to the surface of the plate (z-direction). This transducer was used as a trigger to turn the data recorder on at the proper time, thus assuring that the acceleration at the response point would be measured during the appropriate time period. Two accelerometers, a PCB 306A02 triaxial on the front and a PCB 302A2 single axis on the back, were used to measure acceleration levels at the response point. The

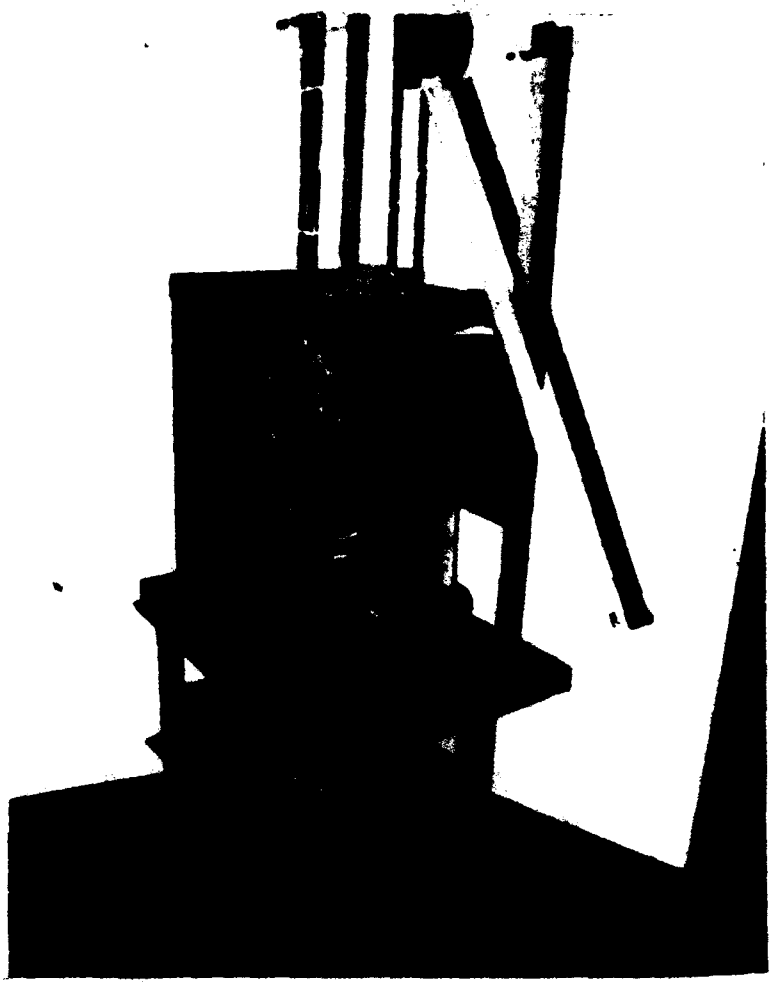

Figure 4. Test stand and impacting mechanism.

acceleration data was collected through a PCB 483B03 power supply and recorded with a Kontron WW700 data acquisition computer. There were no filters added into the data acquisition system although the accelerometers contained 5-kHz low-pass filters. According to the manufacturer, both models of accelerometers have a rise time of about 10 μs with a range of about 1,000 g's and a resolution of 0.01 g's. The single-axis accelerometer had a resonant frequency of 30 kHz, and the triaxial accelerometer had a resonant frequency of 8 kHz. A schematic of the data acquisition system is shown in Figure 5.

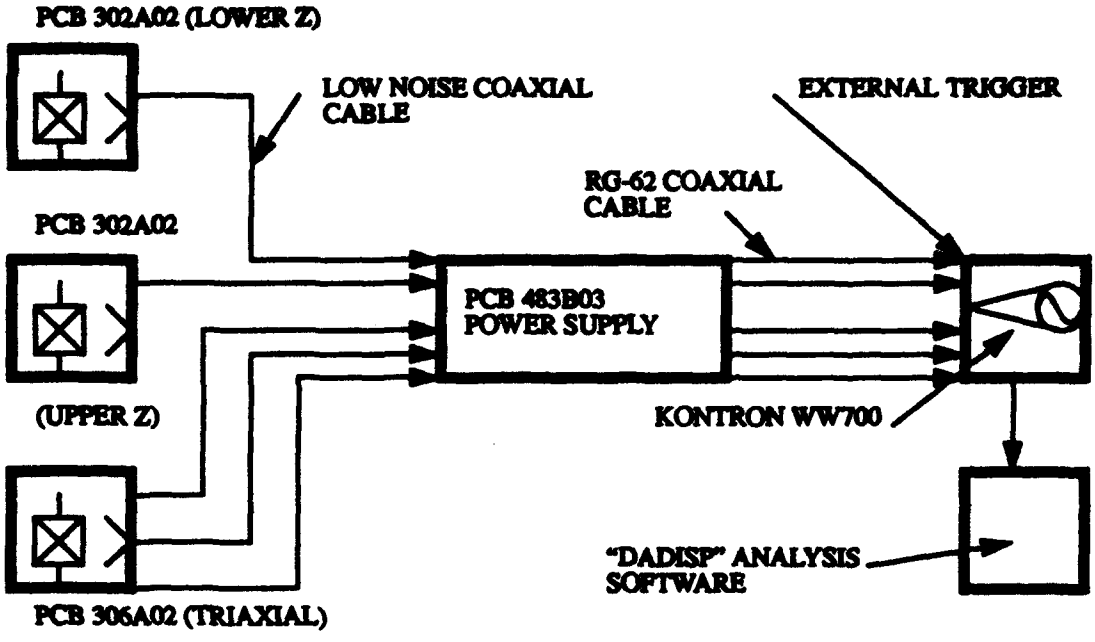

Figure 5. Schematic of data acquisition system.

5. EXPERIMENTAL PROCEDURE

The first step in the experimental procedure was to mount the selected target plate in the test stand. The plate was positioned so that the ball bearing would impact at the marked center point of the plate. The plate would then be clamped in place along the bottom edge using a piece of flat stock and two c-clamps. The c-clamps were always torqued at 11.3 N–m (100 lbf-in). Next, the radial angle bracket would be positioned at the top edge of the plate, a piece of rubber was inserted between the plate and the bracket, and the plate was clamped to the bracket using two c-clamps. The angle bracket was then secured to the test stand by tightening the nuts on the two threaded studs that protruded through the radial slots of the test stand.

Once the target plate was mounted, the accelerometers were fastened to the plate, making use of the threaded mounting holes. Then the instrumentation cables were connected, and the power supply was activated. The power supply was always allowed to warm up for a few minutes before experimentation commenced.

Each target plate was impacted by the ball bearing which was dropped from three different heights. These three heights corresponded to 30°, 45°, and 60° increments as measured by the protractor that was part of the release mechanism. The three drop heights are also referred to as loads in this document. Loads one, two, and three correspond to the 30°, 45°, and 60° increments mentioned previously. Generally, five experiments were conducted for each drop height. The five repetitions were conducted in an attempt to gain confidence in the resulting data.

Prior to each impact experiment, the data acquisition system was "armed" so that data for the next impact on the target plate would be recorded. This "arming" process was simply a matter of pushing the trigger button on the Kontron computer. At this point, the video camera was activated, and the ball bearing was then released.

Once the impact occurred, the acceleration vs. time data for each channel was immediately displayed on the Kontron's screen. Five channels of data were recorded for each impact. The five channels included the z-direction acceleration behind the impact point, the z-direction acceleration at the response point, and the x-, y-, and z-direction accelerations measured at the response point by the triaxial accelerometer. The data sampling rate was 1 data point per microsecond, and 1,000 data points were recorded for each channel. Once the data was recorded, it was downloaded to floppy disks for future analysis.

6. COMPUTATIONAL PROCEDURE

The Automatic Dynamic Incremental Nonlinear Analysis (ADINA) finite element program was used to conduct the computational portion of this effort. ADINA-IN was used as the preprocessor program, and ADINA-PLOT was utilized for post processing. Information required by ADINA to run the desired computations included plate geometries, material properties, time step between calculations, number of time steps, boundary conditions, duration and direction of impact, peak force of impact, and the locations of the impact point and the response point. The plate geometries were simply the same as the actual

plates used in the experiments. The material properties used were as presented earlier. The time step chosen was 1 μs. This matched the experimental sampling rate and was smaller than the time step recommended by ADINA which is calculated by using the following formula:

$$\Delta t = \frac{L}{C} = L\sqrt{\frac{\rho}{E}} \quad , \tag{1}$$

where

L = distance between nodes,

C = speed of sound through material,

ρ = density of material, and

E = modulus of elasticity.

For mild steel, Δt was calculated to be 3.82×10^{-6} s, and for 5083 aluminum 3.7×10^{-6} s was calculated. Thus, 1×10^{-6} was of the same order of magnitude but provided better resolution in the calculations.

The peak force was calculated by using the impulse equation as shown in University Physics (Sears, Zemansky, and Young 1978). The equation is as follows:

$$\int_t^{t1} F(T)\, dT = m\,(v_i - v_f) \quad , \tag{2}$$

where

F = total force from impact,

m = mass of the impactor,

v_i = striking velocity, and

v_f = rebound or final velocity.

The two velocities are found by energy balance equations. From Walton (1985), the loading or forcing function for a ball bearing impact is a half-sine wave function. Dobyns (1981) provides the form of such a function as follows:

$$F(t) = F_o \sin(at) , \tag{3}$$

where

F_o = peak force, and

$a = \pi/t_1$.

Thus, if t = 0, solving equation 2 gives:

$$F_o = \frac{\pi m (v_i - v_f)}{2t_1} , \tag{4}$$

where in this case t_1 represents the duration of impact.

The duration of impact was calculated by the equation given by Greszczuk (1982) and is as follows:

$$t_1 = 2.94 \left(\frac{5}{4mnv^{1/2}} \right)^{\frac{2}{5}} , \tag{5}$$

where

$$n = \frac{4\sqrt{R_1}}{3\pi (K_1 + K_2)} , \; K = \frac{1 - \nu^2}{\pi E} , \tag{6}$$

and

$$m = \frac{1}{m_1} + \frac{1}{m_2} , \tag{7}$$

where

m_1 = mass of ball bearing,

m_2 = mass of plate,

v = striking velocity,

R_1 = radius of ball bearing,

K_1 = K for ball bearing material,

K_2 = K for plate material, and

ν = Poisson's ratio.

Impact durations were calculated for each of the three striking velocities corresponding to the three drop heights and each plate material. These durations are tabulated in Table 2.

Table 2. Calculated Impact Durations

Angle of Ball Bearing Drop (°)	Impact Duration for Mild Steel Plate (s)	Impact Duration for Aluminum Plate (s)
30	81.22×10^{-6}	106.12×10^{-6}
45	75.08×10^{-6}	98.10×10^{-6}
60	71.19×10^{-6}	93.03×10^{-6}

Calculated peak forces (F_o) for representative experiments for each load and plate combination are presented in Table 3.

Table 3. Calculated Peak Forces Based on Experimental Rebound Height

Plate Material and Angle (°)	Load 1 (30° drop), F_o, (N)	Load 2 (45° drop), F_o, (N)	Load 3 (60° drop), F_o, (N)
MS 0	3,350	5,200	7,170
MS 30	3,275	4,950	7,050
MS 60	3,250	4,975	7,030
MS 90	3,160	5,108	7,080
MS 120	3,250	5,148	7,105
AL 0	2,300	3,575	4,910
AL 30	2,219	3,450	4,850
AL 60	2,300	3,450	4,930
AL 90	2,250	3,500	4,965
AL 120	2,280	3,550	5,075

The rebound height of the ball bearing after impact was an important factor in the calculation of the peak force. It should be noted that the height of the ball as seen by the video camera was adjusted to account for the ball bearing and camera not being at the same height. For example, if the video camera was positioned lower than the ball bearing, the rebound height as measured on the grid board would be high. Knowing the height of the camera in relation to the grid board and the ball bearing and the horizontal distance between the three, it was a simple geometry problem to determine the actual rebound height. Figure 6 presents this pictorially.

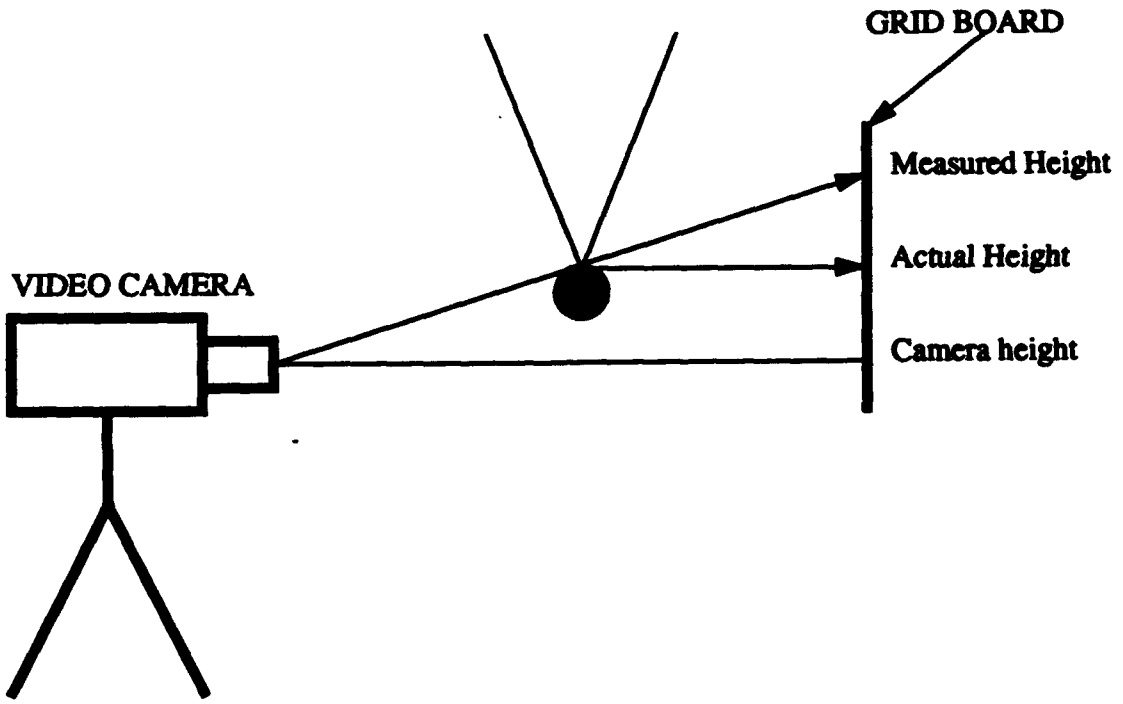

Figure 6. The difference between measured and actual rebound height.

For modeling purposes the impact was assumed to be linear elastic, and shell elements were used to build the plate geometries. Shell elements were selected primarily due to the fact that an original intent was to look at plates that were quite thick. The ADINA theory manual (ADINA R&D, Inc. 1987) states that plate elements can be employed to model thin plates, and shell elements can be used for thick or thin plates. In keeping with the objective of determining whether simple finite element models could be used to determine shock attenuation, there was no attempt at modeling weld geometries and materials. Appendix A contains example of ADINA-IN and ADINA-PLOT files that had to be generated along with some sample outputs.

7. EXPERIMENTAL RESULTS

It was decided that, for this effort, the acceleration at the response point normal to the surface of the plate as measured on the back side of the plate was the parameter of interest. This was primarily due to the fact that shock-sensitive components in armored combat vehicles are mounted inside the vehicle (back side of armor) and that the normal or z-direction would see the largest deflections. The triaxial accelerometer on the front side of the plate was used to assure the reliability of the single-axis accelerometer.

When the results were first gathered for the 12.7-mm steel plates, it was noticed that the results from the 30° and 90° plates yielded acceleration levels that were significantly higher than for the other plates. This phenomenon raised serious concerns about the experimental design, welding techniques, etc., and it did not fall into the expected trend. To investigate further, additional plates joined at 15°, 45°, and 75° were manufactured and tested. The results from the new plates followed the expected trend and agreed with the 0°, 60°, and 120° plates. At this point, new 30° and 90° plates were fabricated and tested with more favorable results. The aluminum plates were tested after the steel plates, and the 90° plate was refabricated due to the same phenomenon as before.

Figures 7–11 are a set of acceleration-vs.-time plots for the response point as measured by the single-axis accelerometer. These plots were made through the use of a signal processing program called "DADISP." The plots presented are for the mild steel plates impacted by Load 1 (30° ball bearing drop). Note that the shape of each plot is similar regardless of the plate geometry. This similarity also held true for the aluminum plates. Also note that these plots only present the acceleration data out to approximately 100 μs. This was due to the fact that beyond this point, reflections off of the plate edges were expected to reach the response point. Thus, the largest amplitude in the presented time domain was used as the defining acceleration level for each case. All other sets of plots were similar and, therefore, are not presented in this document. The defining acceleration levels for each target and impact load condition experiment are summarized in tabular form in Appendix B. Also of interest was the timing of the signal arrival at the response point for the 120° plate as compared to the other plates. In all experimental cases, the 120° plates witnessed accelerations at the response point earlier than the other plates, all of which had similar timing. At this point in time, no explanation of this phenomenon can be offered. A discussion of signal arrival time as compared to speed of sound travel through the plate materials will be presented in the computational results section.

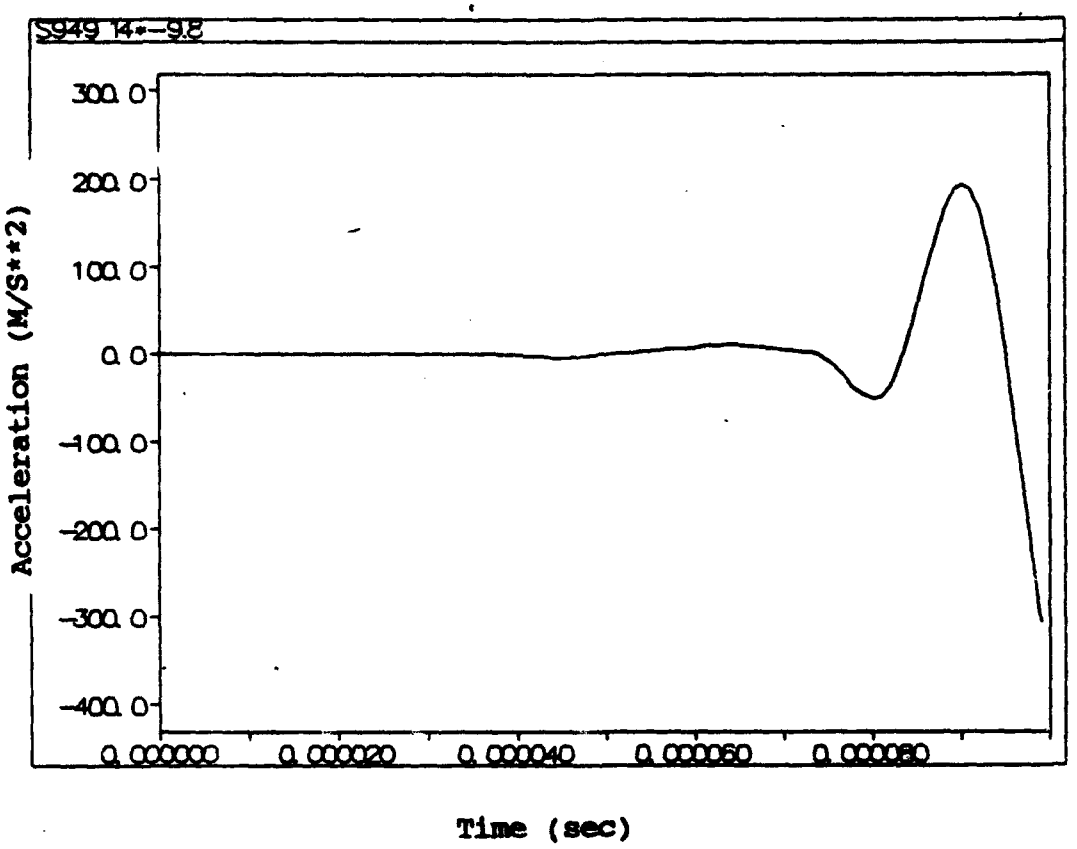

Figure 7. Acceleration vs. time for 0° mild steel plate subjected to load 1.

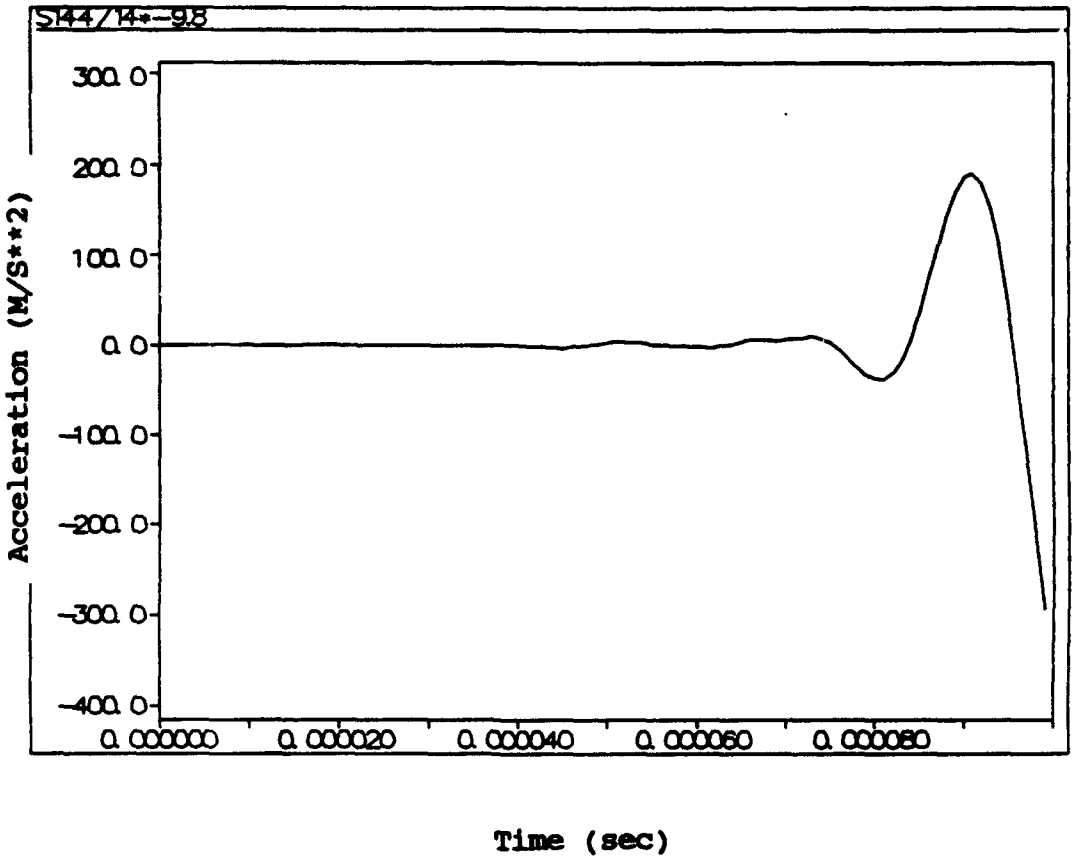

Figure 8. Acceleration vs. time for 30° mild steel plate subjected to load 1.

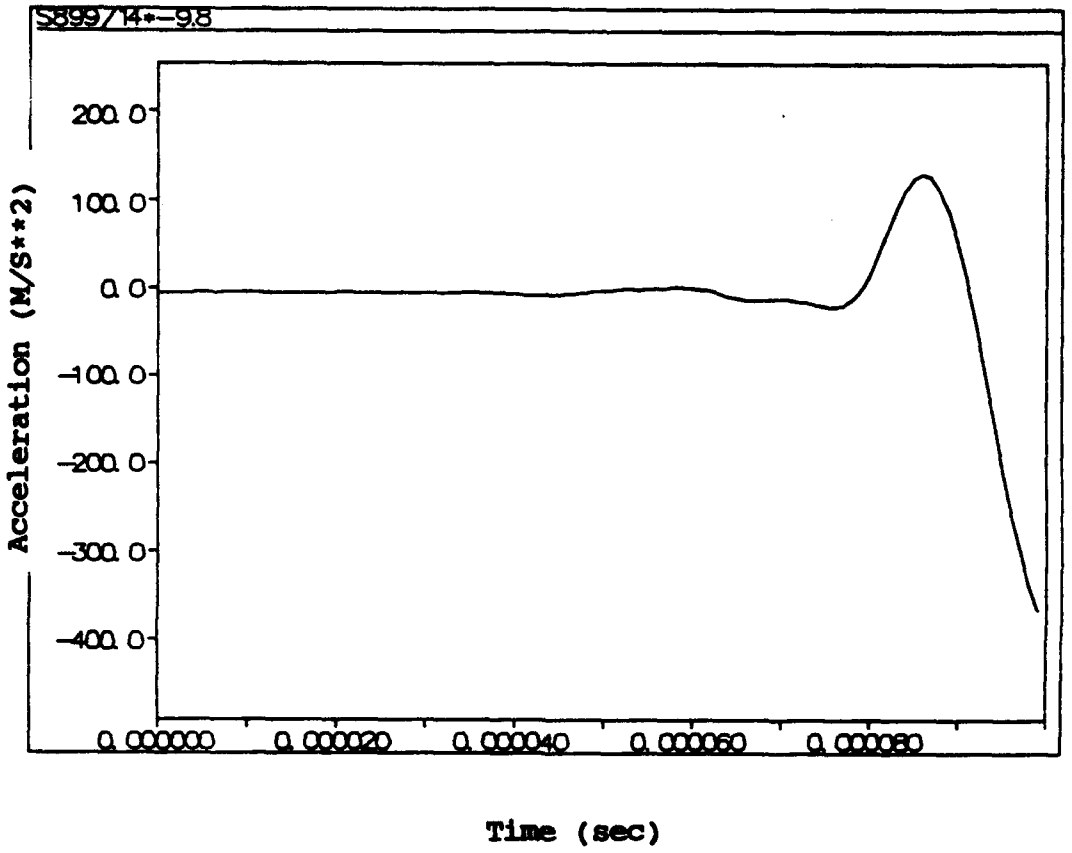

Figure 9. Acceleration vs. time for 60° mild steel plate subjected to load 1.

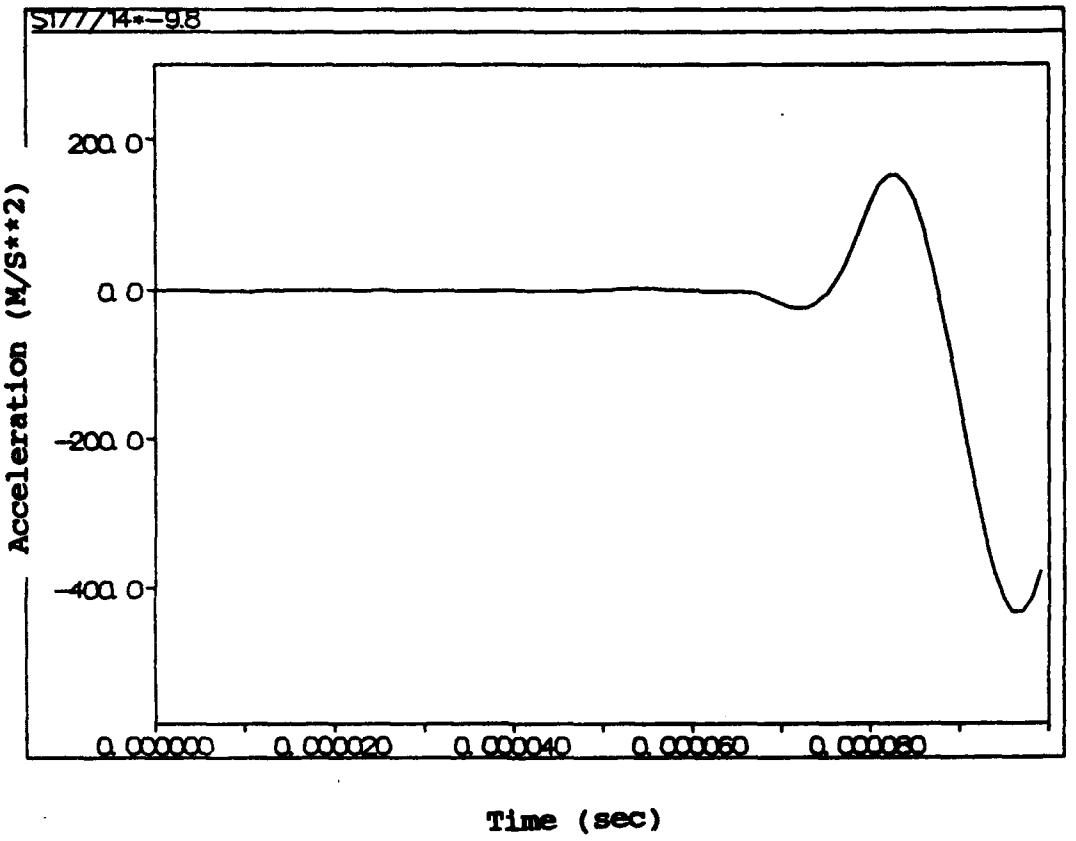

Figure 10. Acceleration vs. time for 90° mild steel plate subjected to load 1.

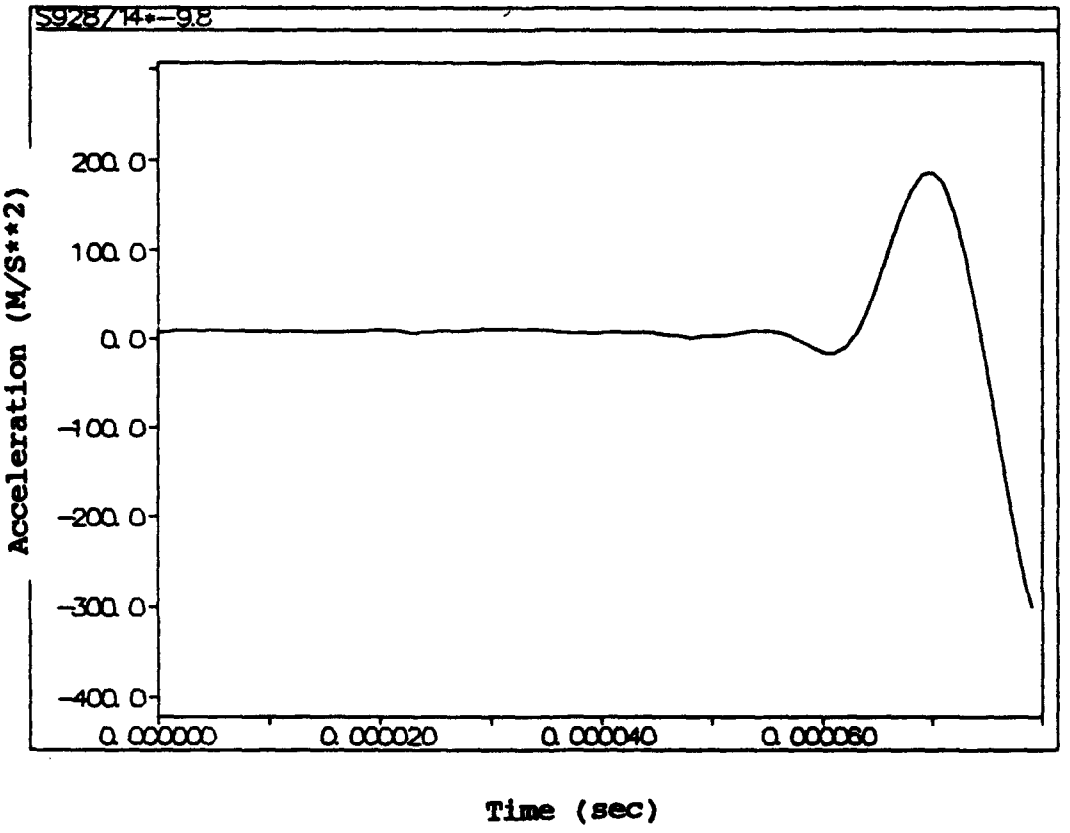

Figure 11. Acceleration vs. time for 120° mild steel plate subjected to load 1.

8. COMPUTATIONAL RESULTS

Once the rebound heights were obtained, there was sufficient information available to conduct the computational analysis. Results were plotted and tabulated, for the response point, for each of the impact and plate configuration combinations. Sample plots of the normal acceleration vs. time are provided in Figures 12–16. Note that there is always a small dip in the record prior to the positive increase in acceleration as was the case with the experimental data records.

The time at which the response point began to see accelerations was important as far as validating the computations was concerned. The time at which the accelerations went positive for the first time corresponded to the time it would take to travel 30.5 cm (1 ft) through the steel or aluminum at the speed of sound. It was felt that this was a good check to determine if the finite element code was working properly. The computations were stopped at 86 μs because that was the estimated time of arrival at the response point for the first reflection off of a plate edge. As it turned out, the peak of the first positive hump in the acceleration data appeared to be the defining acceleration level. Thus, there was good agreement between the experimental and computational data as far as determining which point from the acceleration data to use for comparison of the various plates.

The calculated peak acceleration values for each plate and load combination are presented in Table 4. It was interesting to note that the computed peak values for the steel plates matched up with the experimental data quite well while the results for the aluminum plates were not in agreement. The computational values for the aluminum plates were consistently off from the experimental data, thus raising the thought that a multiplicative factor such as coefficient of restitution should have been incorporated into the loading function for the aluminum plate calculations. The lack of a restitution coefficient, however, turned out not to be a problem in that the attenuation functions for the experimental and computational results ended up being very similar. The attenuation functions will be discussed in detail in the following analysis section.

Table 4. Computed Acceleration Values for Each Plate and Load Combination

Plate/Load	0° (m/s^2)	30° (m/s^2)	60° (m/s^2)	90° (m/s^2)	120° (m/s^2)
ms/1	222.7	205.0	192.8	187.1	200.8
ms/2	342.4	309.9	295.3	302.0	317.5
ms/3	476.7	441.3	417.2	419.3	439.1
al/1	409.2	372.3	361.3	346.7	361.9
al/2	636.1	577.4	541.9	539.3	564.7
al/3	873.6	811.6	774.4	765.0	807.3

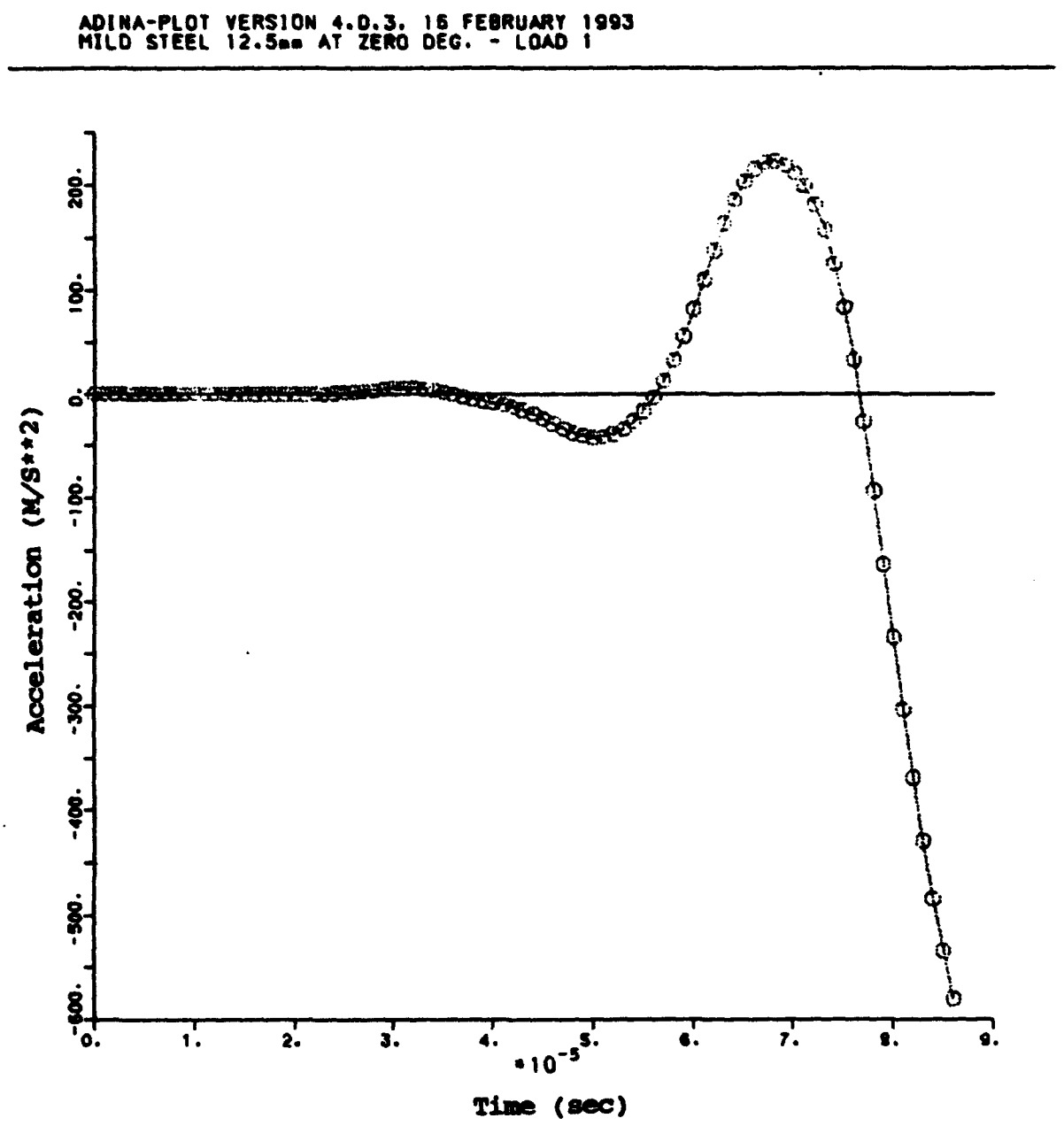

Figure 12. Acceleration vs. time from ADINA for 0° mild steel plate subjected to load 1.

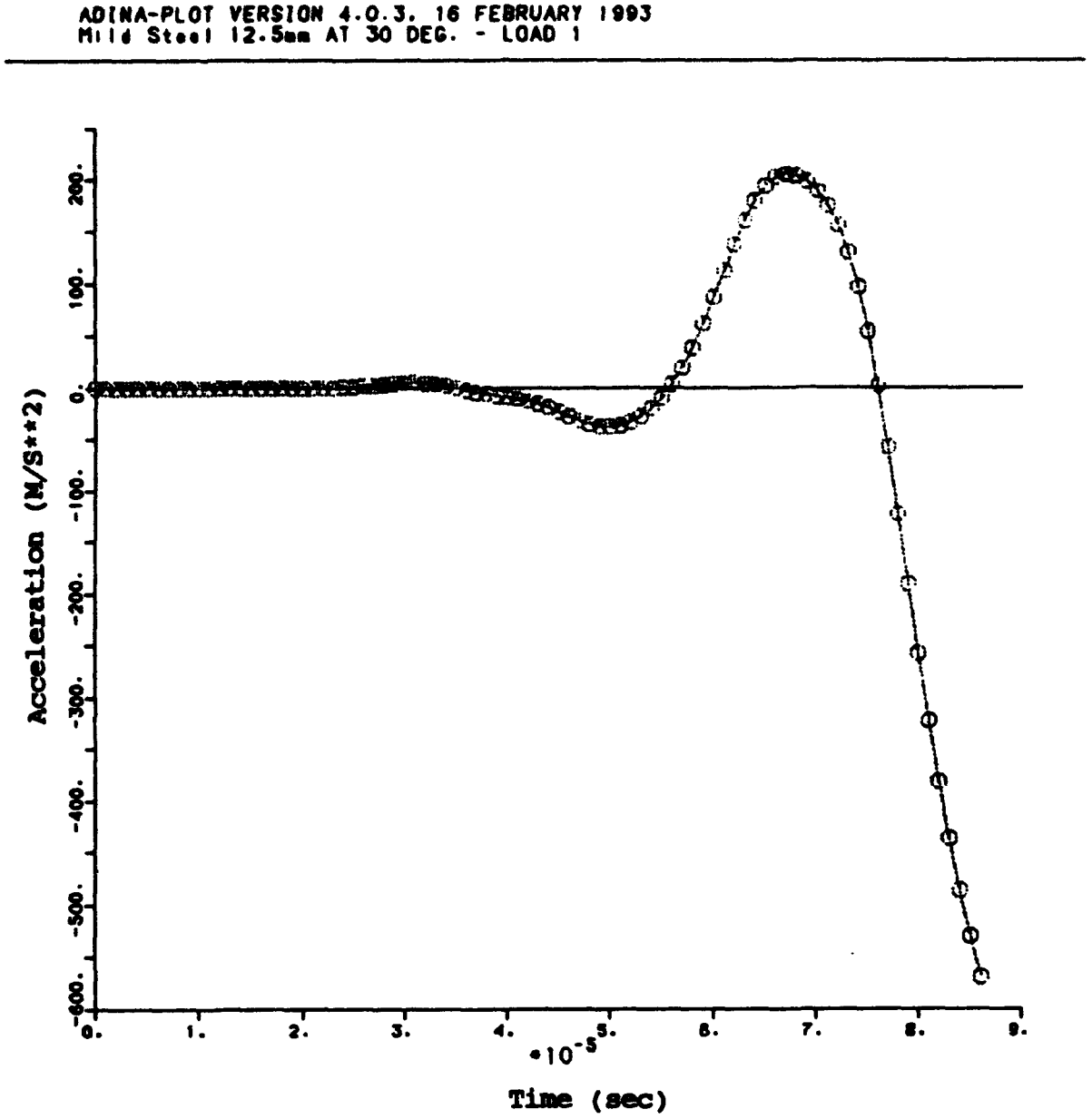

Figure 13. Acceleration vs. time from ADINA for 30° mild steel plate subjected to load 1.

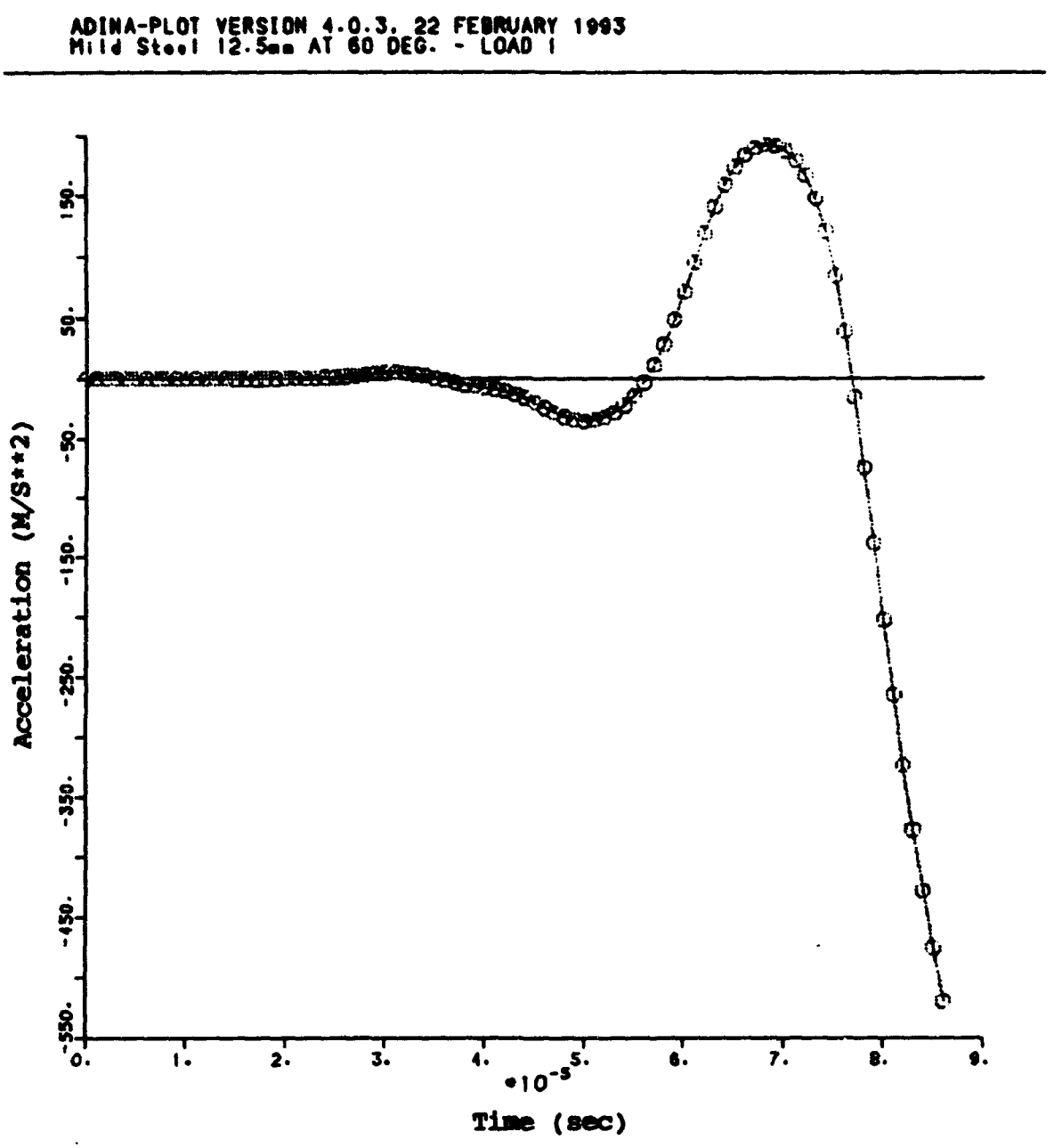

Figure 14. Acceleration vs. time from ADINA for 60° mild steel plate subjected to load 1.

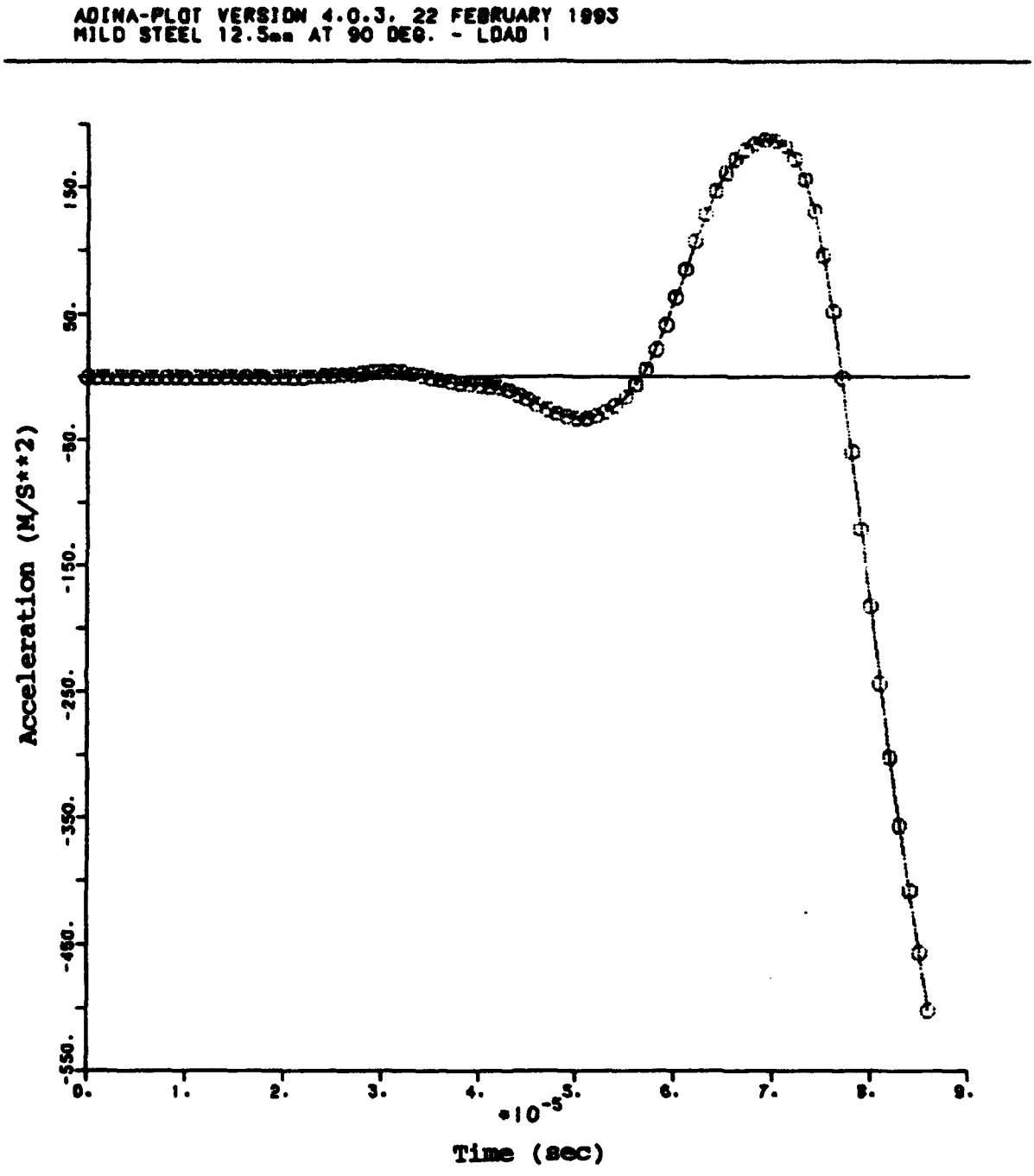

Figure 15. Acceleration vs. time from ADINA for 90° mild steel plate subjected to load 1.

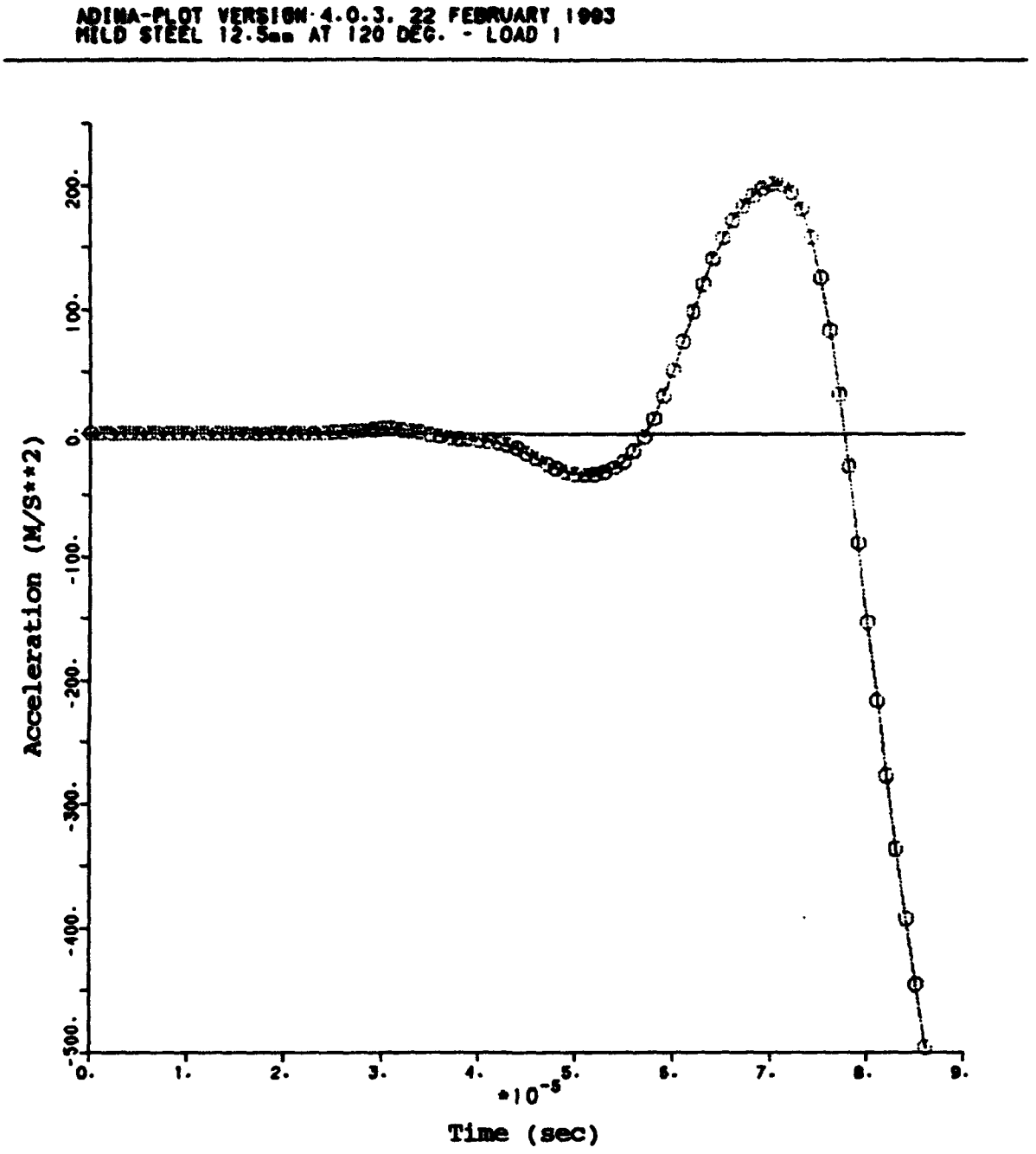

Figure 16. Acceleration vs. time from ADINA for 120° mild steel plate subjected to load 1.

9. ANALYSIS

The tabulated experimental data as shown in Appendix B and computational data were downloaded to a personal computer where a program called "SYSTAT" was used for analysis of the results. The first step in the analysis was to verify that there was in fact a relationship between the acceleration at the response point and the angle at which the plates were joined. Using linear regression, a straight line was fitted to the data for each set of plates and impact condition. Although the straight line did show that there was a relationship between angle and acceleration, the fit to the data was not good. The next step was to attempt to fit a polynomial function to the data. A quadratic polynomial was attempted first and showed good signs of improvement in that more of the variation in acceleration levels, as presented by the polynomial function, was explained by the variation in plate angles. This was shown by a statistic called the squared multiple correlation (R^2) or correlation coefficient (R) (Miller and Freund 1977). R^2 is the ratio of the variation of the regression sum of squares for a given regression model to the variation of the total sum of squares for a given data set. The closer this ratio is to unity, the more efficient the model is at prediction. This ratio is given in the following equation:

$$R^2 = \frac{\sum\left(\hat{y}_i - \bar{y}\right)^2}{\sum\left(y_i - \bar{y}\right)^2}, \tag{8}$$

where

$\hat{y}_i$ = model predicted values,

$\bar{y}$ = grand mean of data set, and

y_i = experimental data points or observations.

The R^2 values were quite good for fourth-order polynomial function, but the shape of these functions was counterintuitive. The quadratic functions were adopted due to the shape of the fourth-order functions and the fact that quadratic polynomials fit the computational data extremely well. The fourth-order polynomial equations are presented in Appendix C for completeness.

Once the equations for acceleration were determined, they had to be converted into equations for attenuation. The acceleration equations were solved for the case where the angle is 0°. The acceleration

equations were then divided by the values obtained at 0° to obtain the attenuation equations. This equation can be represented by the following:

$$\text{Attenuation} = \frac{\text{Acceleration } (\alpha)}{\text{Acceleration } (0)} . \tag{9}$$

The quadratic acceleration and attenuation equations follow with their respective R^2 values (equations 10–16). The best R^2 value (0.592) for the mild steel plates was achieved for the largest impacting load. The R^2 value was higher for the aluminum plates for the fourth-order polynomial fit and was lower for the quadratic approximations. As mentioned earlier, the R^2 value was almost 1.0 for all of the computational results which was expected since the computations did not include the effects of welds or variation of impact force from one drop to the next. Note that the R^2 values are quite low for the experimental data fits. Since the equations below are broken out separately for load and material types, the low R^2 values indicate that there are other parameters that affect the level of acceleration as much as or more than the plate angles. Of the other parameters, pure experimental error and the welds are suspected to be major contributors. In addition to the R^2 statistic, there are other measures that could have been applied, for example, to show how much of the total possible variation in acceleration due to plate angle was actually explained by the quadratic functions.

Mild Steel: Load1: $R^2 = 0.142$

$$\begin{aligned} \text{ACC} &= 180.6 - 51.5\,(\text{ANG}) + 19.1\,(\text{ANG})^2; \\ \text{ATT} &= 1 - 0.285\,(\text{ANG}) + 0.106\,(\text{ANG})^2. \end{aligned} \tag{10}$$

Mild Steel: Load2: $R^2 = 0.445$

$$\begin{aligned} \text{ACC} &= 419.8 - 200.3\,(\text{ANG}) + 78.1\,(\text{ANG})^2; \\ \text{ATT} &= 1 - 0.477\,(\text{ANG}) + 0.186\,(\text{ANG})^2. \end{aligned} \tag{11}$$

Mild Steel: Load3: $R^2 = 0.592$

$$\begin{aligned} \text{ACC} &= 721.2 - 468.5\,(\text{ANG}) + 208.6\,(\text{ANG})^2; \\ \text{ATT} &= 1 - 0.650\,(\text{ANG}) + 0.289\,(\text{ANG})^2. \end{aligned} \tag{12}$$

Aluminum: Load1: $R^2 = 0.243$

$$ACC = 183.3 - 64.6\,(ANG) + 28.4\,(ANG)^2;$$
$$ATT = 1 - 0.352\,(ANG) + 0.155\,(ANG)^2. \quad (13)$$

Aluminum: Load2: $R^2 = 0.137$

$$ACC = 349.7 - 81.0\,(ANG) + 26.1\,(ANG)^2;$$
$$ATT = 1 - 0.232\,(ANG) + 0.075\,(ANG)^2. \quad (14)$$

Aluminum: Load3: $R^2 = 0.309$

$$ACC = 513.7 - 218.8\,(ANG) + 114.9\,(ANG)^2;$$
$$ATT = 1 - 0.426\,(ANG) + 0.224\,(ANG)^2. \quad (15)$$

ADINA computations for both materials and all three loads resulted in virtually the same equations with R^2 values ranging from 0.971 to 0.999. The attenuation equation based on the computational data follows:

$$ATT = 1 - 0.2\,(ANG) + 0.08\,(ANG)^2 \quad (16)$$

Figures 17–22 are plots of the quadratic acceleration equations and the associated experimental data for each impact load. Figures 23 and 24 show the quadratic acceleration equations and associated acceleration data from ADINA. Note that as the R^2 values suggest, the quadratic equations fit the computational data very well. Finally, Figures 25 and 26 contain plots of the attenuation functions for the computational and experimental results. Note that only one equation is plotted for the computational data because the equation was virtually identical for all three load conditions. The attenuation factor that one would obtain from these plots or through the use of the equations is a multiplication factor for the peak acceleration as the shock crosses a welded joint. Thus, a factor of 0.8 means that the acceleration is attenuated by 20%. The attenuation function plots and equations should not be used for angles beyond 120°. It is unknown, at this time, how well extrapolations beyond the limits of the experimental data would predict attenuation.

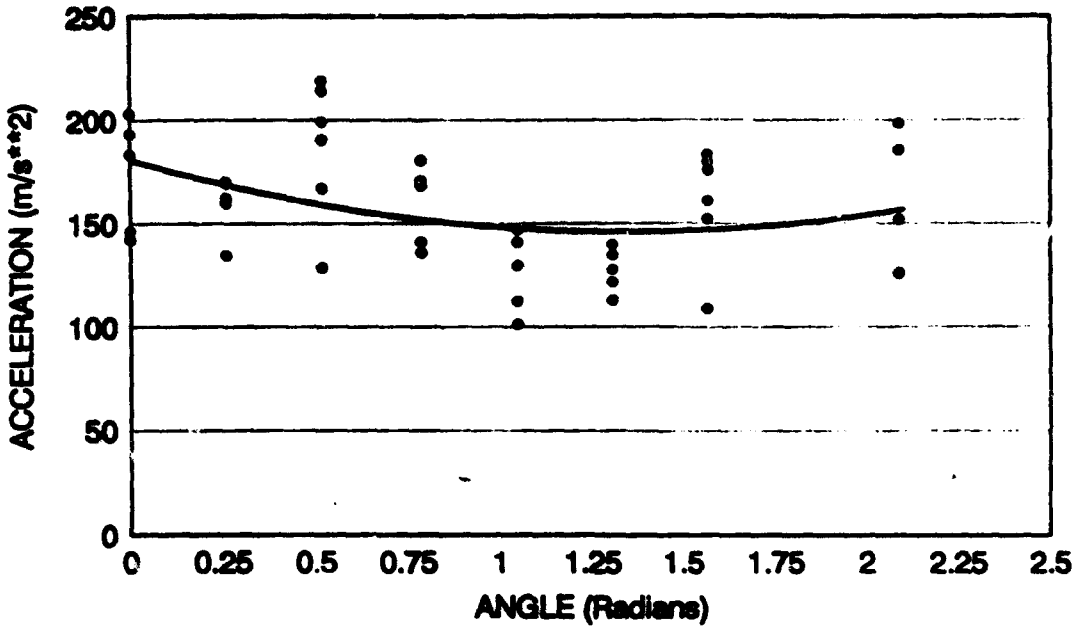

Figure 17. Quadratic function fitted to experimental data for mild steel plates subjected to load 1.

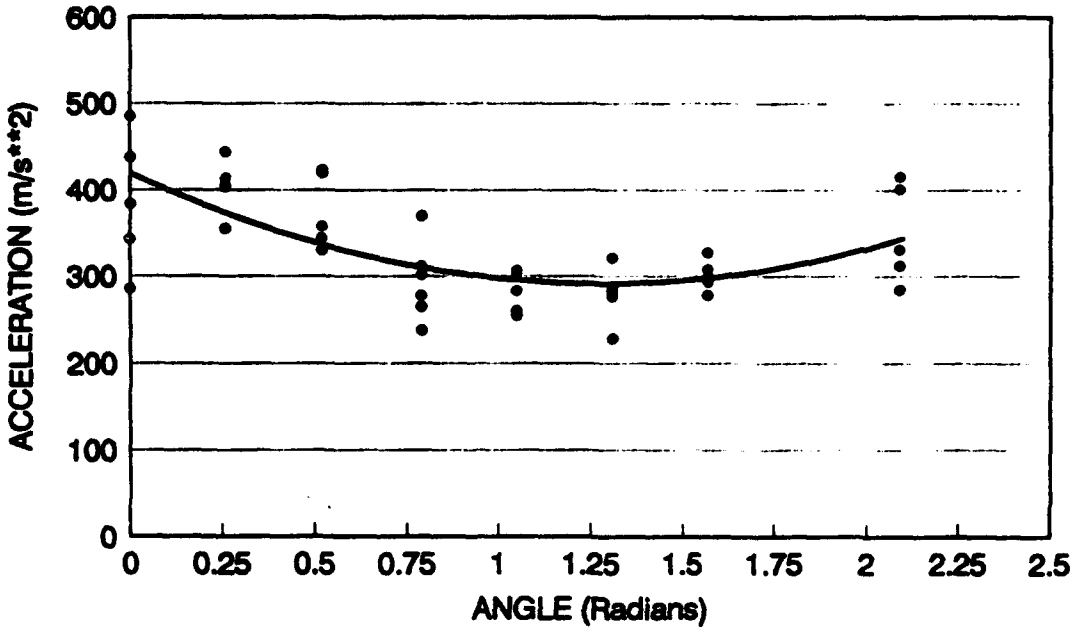

Figure 18. Quadratic function fitted to experimental data for mild steel plates subjected to load 2.

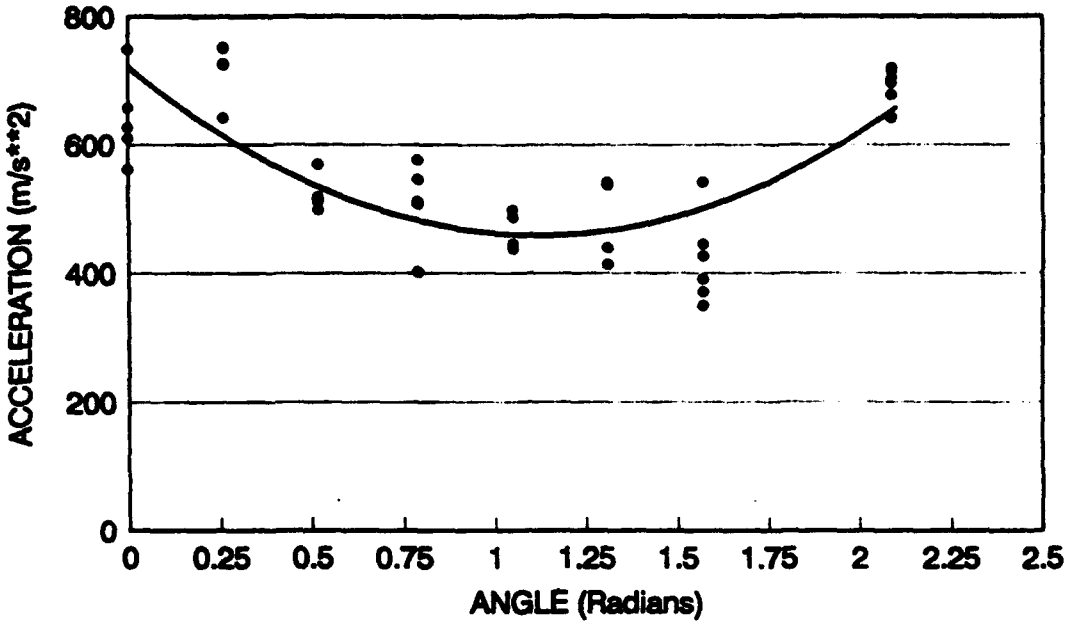

Figure 19. Quadratic function fitted to experimental data for mild steel plates subjected to load 3.

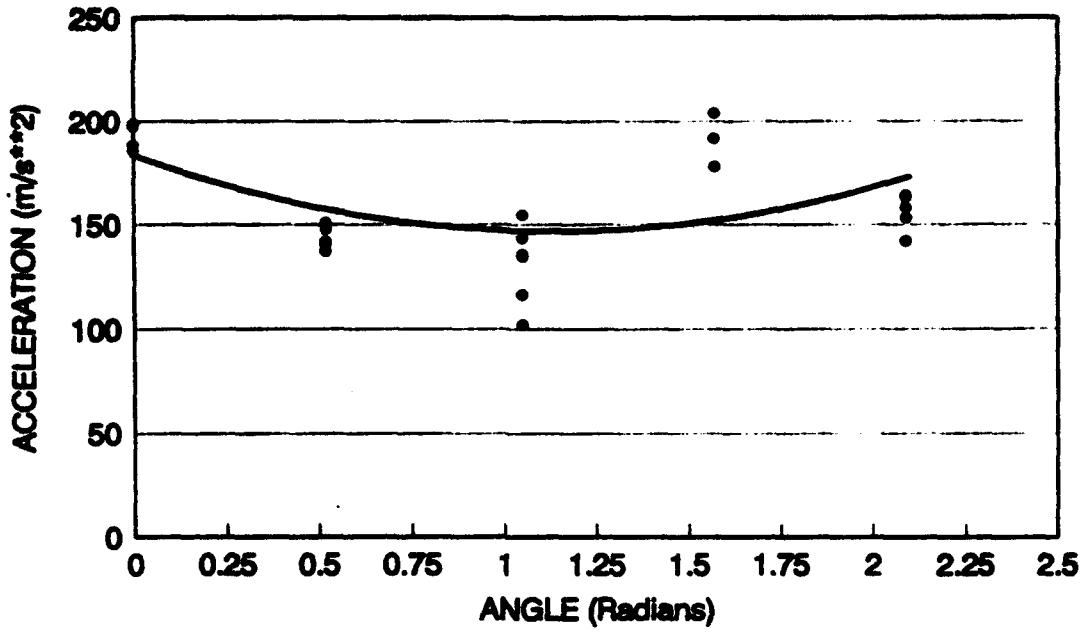

Figure 20. Quadratic function fitted to experimental data for 5083 aluminum plates subjected to load 1.

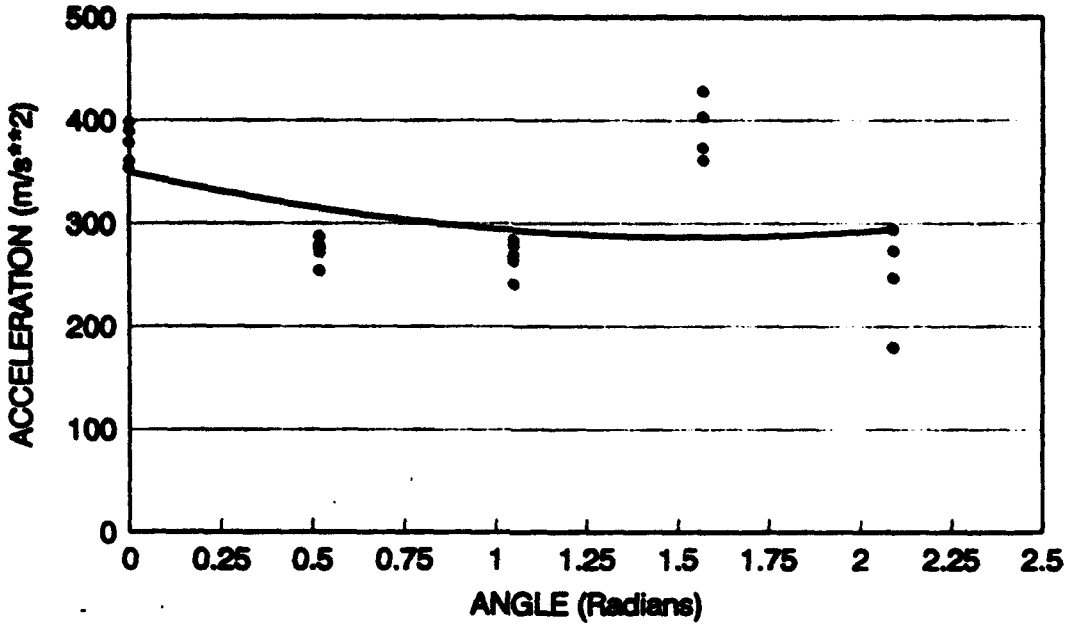

Figure 21. Quadratic function fitted to experimental data for 5083 aluminum plates subjected to load 2.

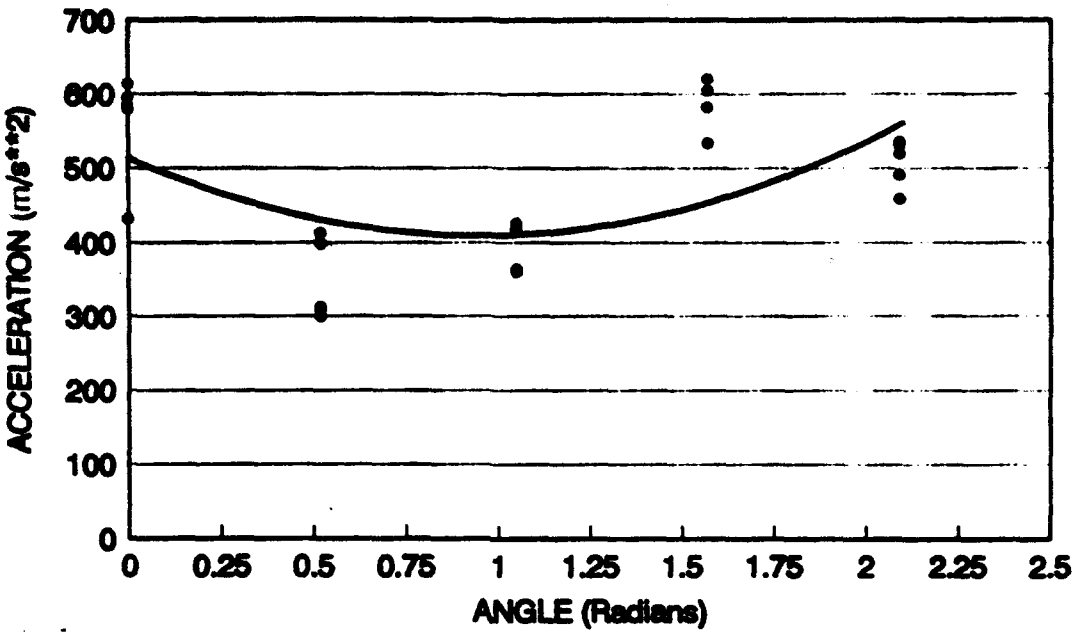

Figure 22. Quadratic function fitted to experimental data for 5083 aluminum plates subjected to load 3.

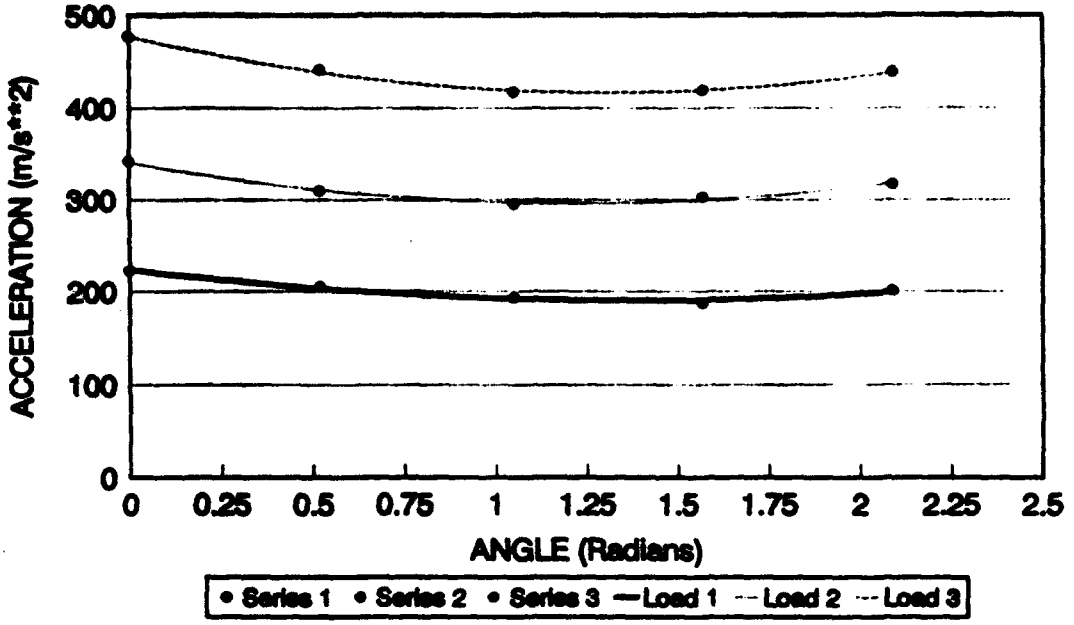

Figure 23. Quadratic functions fitted to computational data for mild steel plates subjected to all three loads.

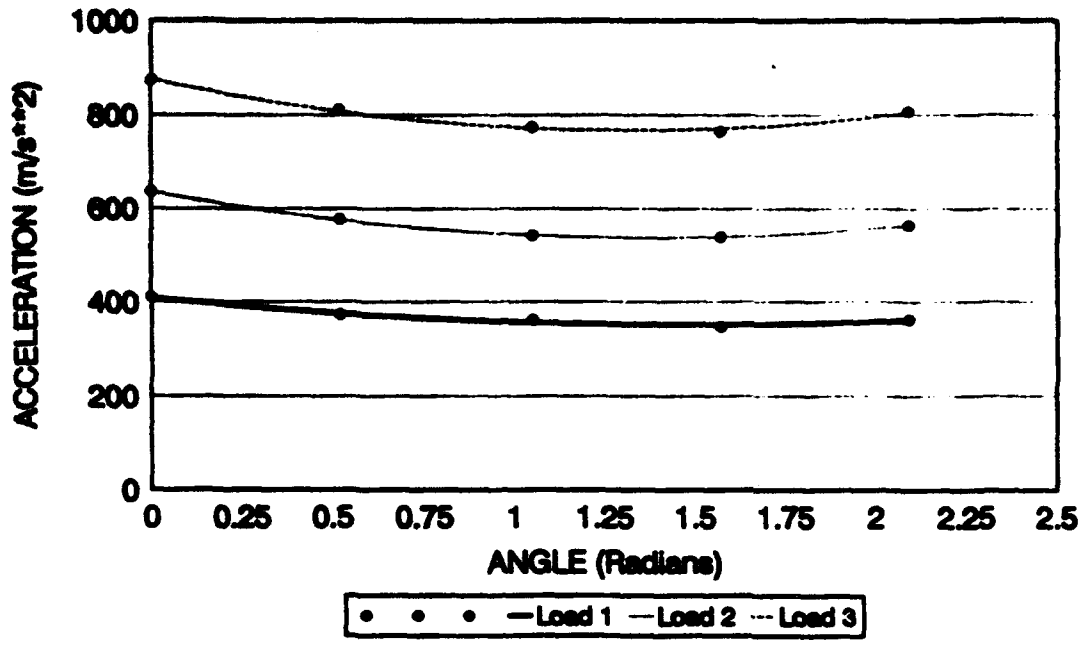

Figure 24. Quadratic functions fitted to computational data for 5083 aluminum plates subjected to all three loads.

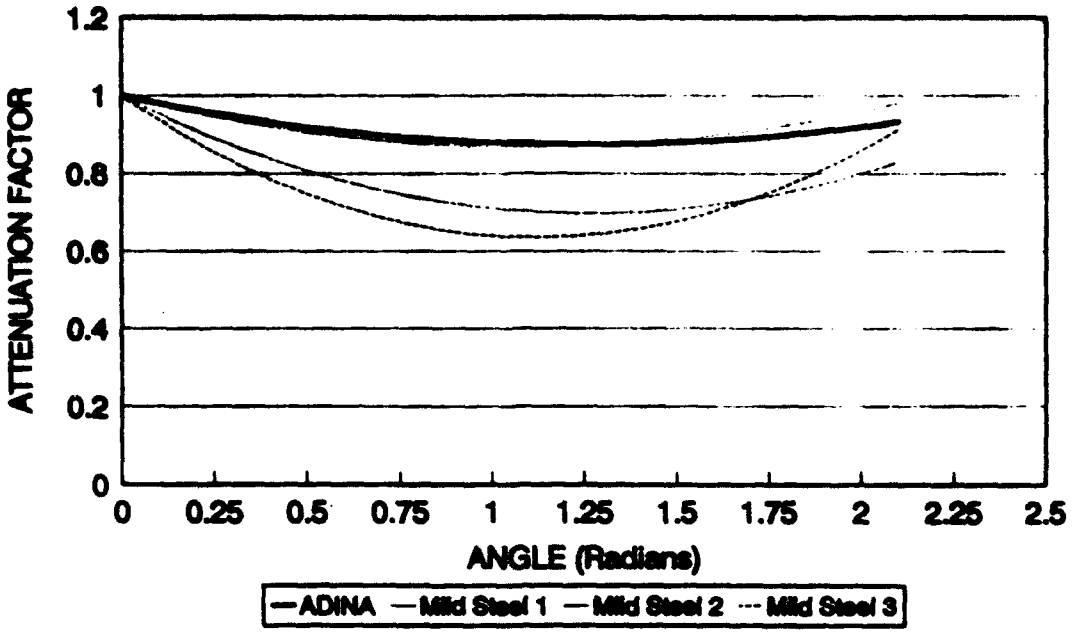

Figure 25. Attenuation functions for mild steel plates.

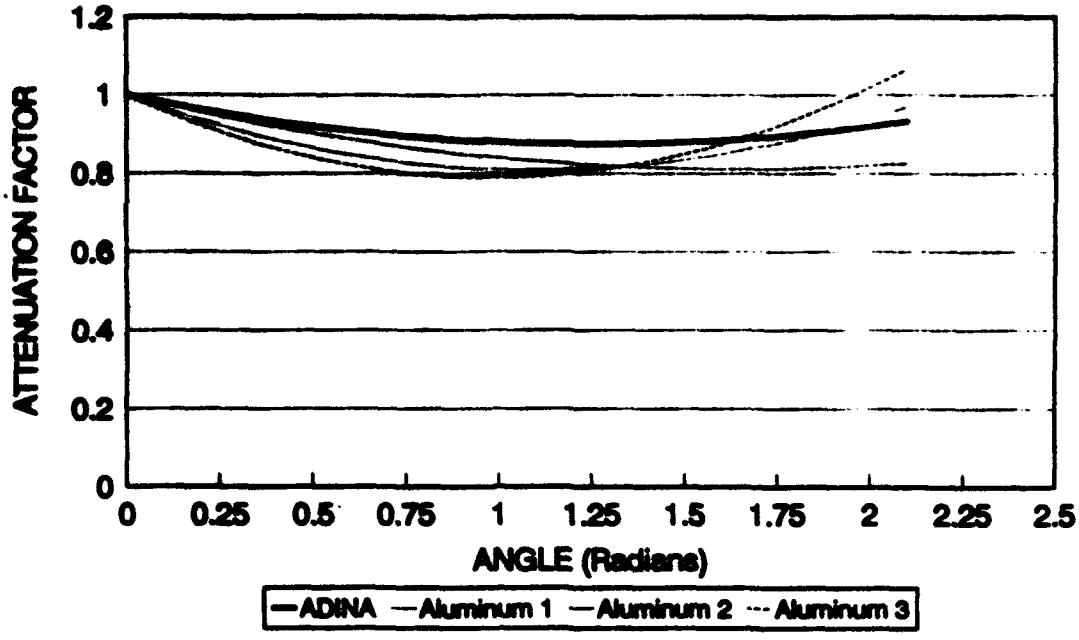

Figure 26. Attenuation functions for 5083 aluminum plates.

Upon review of the two attenuation plots, one should note several points. The attenuation functions for the aluminum plates are very similar regardless of the impact load. For the mild steel plates, the functions spread out somewhat for the different loads, but at any given angle the attenuation function does not appear to vary more than about 25%. Also of interest here are the computationally derived attenuation functions that appear to be flatter than the experimentally derived functions and which did not show any effect of load variation. This is perhaps due to the welds not being accounted for in the computations and to some experimental variation in the impact loads. A final point to mention is the fact that the computations from ADINA showed no difference in the angle attenuation functions for the mild steel and aluminum plates. This is not a surprise in that an elastic model was used, distance to the response point was held constant, and welds were not incorporated. Thus, the only remaining parameter that could have an effect on shock attenuation was the angle formed by the plates.

10. CONCLUDING REMARKS AND FUTURE WORK

Experimental and computational analyses were performed to determine if angle variation between welded armor plates has an effect on shock attenuation. As a result of this effort, it has been shown that there is an effect, and attenuation functions have been provided for three impact conditions and two material types. These functions are given in equations 10–16. It is interesting to note that Barrett and Kacena (1972) also looked at joint attenuation and came up with a conservative estimate of 40 percent across a flat bolted joint. This bit of information fits in nicely in that one would expect a bolted joint to have a greater attenuation factor than a completely welded joint. Unfortunately, Barrett and Kacena did not investigate the effect of plate angle variation.

The computational work showed that attenuation across the joints was constant over the range of materials and impact conditions. The experimental work showed that the attenuation functions were at least in the same general neighborhood over the range of materials and impact conditions considered. In particular, the attenuation functions provided for the aluminum plates were quite similar for all three impact conditions.

It was shown that simple finite element models could be used to derive attenuation functions that are in the range of functions based on experimental data. However, the fact that data from the experiments was required for derivation of loading functions for the finite element program suggests that one would

have to continue to conduct experiments to obtain the proper loading functions for various impact loads and types of impact.

There is a substantial amount of work that could be conducted to advance further understanding of shock attenuation across joints. A continuation of similar work, as presented in this document, taking acceleration data and transforming it into Shock Response Spectra (SRS) would certainly be worth while since component standards for shock are given in this form. It is recommended that the use of larger target plates be investigated for this purpose. Larger plates are important for this purpose so that the shock could be measured for longer periods of time before reflections from boundaries would interfere. Note that "small" plates were used for this effort since only the very first portion of the shock was analyzed. The question still remains as to whether the first portion of the shock is sufficient for characterization of attenuation effects. Additionally, work including larger impact loads, different impactor shapes, different loading mechanisms such as blast, various welding techniques, additional materials, cast targets that would not require welds, and different joining techniques such as bolting would be of considerable interest. Also, an attempt should be made at improving or changing the experimental setup used for this effort. The purpose here would be to reduce the experimental error which was shown to be high by the R^2 values.

INTENTIONALLY LEFT BLANK.

11. REFERENCES

ADINA R&D, Inc. "ADINA Theory and Modeling Guide." ARD Report 87–8, First Printing, Watertown, MA, 1987.

Barrett, S. "The Development of Pyro Shock Test Requirements for Viking Lander Capsule Components." Institute of Environmental Sciences Proceedings, vol. 2, pp. 5–10, 1975.

Barrett, S., and W. J. Kacena. "Methods of Attenuating Pyrotechnic Shock." Shock and Vibration Bulletin, vol. 42, part 4, pp. 21–32, 1972.

Deitz, P. H., M. W. Starks, J. H. Smith, and A. Ozolins. "Current Simulation Methods in Military Systems Vulnerability Assessment." BRL-MR-3880, U.S. Army Ballistic Research Laboratory, Aberdeen Proving Ground, MD, 1990.

Dobyns, A. L. "Analysis of Simply-Supported Orthotopic Plates Subject to Static and Dynamic Loads." AIAA Journal, vol. 19, no. 5, pp. 642–650, 1981.

Gresczuk, L. B. Impact Dynamics. First Edition. New York: John Wiley and Sons, Inc., 1982.

Klopcic, J. T., M. W. Starks, and J. N. Walbert. "A Taxonomy for the Vulnerability/Lethality Analysis Process." BRL-MR-3972, U.S. Army Ballistic Research Laboratory, Aberdeen Proving Ground, MD, 1992.

Miller, I., and J. E. Freund. Probability and Statistics for Engineers. Second Edition. New Jersey: Prentice-Hall, Inc., 1977.

Sears, F. W., M. W. Zemansky, and H. D. Young. University Physics. Fifth Edition. Reading, PA: Addison-Wesley Publishing Company, 1978.

Walbert, J. N. "A Proposed Method for Incorporating Ballistic Shock Effects in Vulnerability/Lethality Analyses." BRL-MR-3930, U.S. Army Research Laboratory, Aberdeen Proving Ground, MD, 1991.

Walton, W. S. "Characterization of Ballistic Shock." USACSTA-6262, U.S Combat Systems Test Activity, Aberdeen Proving Ground, MD, 1985.

Walton, W. S. "New Ballistic Shock Protection Requirement for Armored Combat Vehicles." 60th Shock and Vibration Symposium, vol. 1, pp. 299–309, 1989.

INTENTIONALLY LEFT BLANK.

APPENDIX A:

SAMPLE ADINA FILES AND OUTPUTS

INTENTIONALLY LEFT BLANK.

This appendix contains a complete set of input and output files and figures for 1 of the 30 ADINA runs required for this effort. This set of files and figures includes the input and output files for ADINA-IN and ADINA-PLOT, a figure of the plate geometry showing element size and node locations, plots of acceleration in meters/second^2 vs. time at the response point, and the acceleration data in tabular form.

ADINA-IN and ADINA-PLOT were run on a Silicon Graphics 310GTX and ADINA was run on a Cray supercomputer. ADINA-IN was used to set up the plate geometry and loading conditions for ADINA. ADINA actually performed the number crunching for each node point, and ADINA-PLOT was used to extract the desired information for the response point.

```
*       INPUT FILE NO. 3
*
FILEUNITS LIST-8 LOG-7 ECHO-7
FCONTROL HEADING-UPPER ORIGIN-LOWERLEFT
CONTROL PLOTUNIT-PERCENT HEIGHT-1.25
WORKSTATION SYSTEM-13 BACKGROUND-WHITE
*
DATABASE CREATE
HEAD 'Mild Steel 12.5mm AT 60 DEG. - LOAD 1'
*
MASTER IDOF-000000 NSTEP-86 DT-0.000001
PRINTOUT VOLUME-MAXIMUM IPRIC-0 IPRIT-0 CARDIMAGE-NO IPDATA-3
PORTHOLE FORMATTED-YES FILE-60
*
COORDINATES
 ENTRIES NODE   X      Y      Z
          1  .1524 -.1524   0.   TO
         13  .1524  .1492   0    TO
         25  .1524  .2993  -.2608   TO
         37 -.1524  .2993  -.2608   TO
         49 -.1524  .1492   0   TO
         61 -.1524 -.1524   0.   TO
         73  .1524 -.1524   0.
 DELETE  73
*
MATERIAL 1 ELASTIC E-.209E12 NU-.3 D-7840.
EGROUP 1 SHELL RESULTS-STRESSES STRESS-GLOBAL
KINEMATICS DISPLACEMENTS-SMALL STRAINS-SMALL
ANALYSIS MASSMATRIX-LUMPED IMODS-0 METHOD-NEWMARK NMODE-10
FREQUENCIES SUBSPACE-ITERATION NEIG-10 NMODE-10 SSTOL-1.E-10 IFPR-1
THICKNESS 1 0.0127
GSURFACE 1 13 49 61 EL1-4 EL2-4 NODES-16
GSURFACE 13 25 37 49 EL1-4 EL2-4 NODES-16
FIXBOUNDRIES DIR-123456 TYPE-LINES
25 37
61 1
SHELLNODESDOF DOF-DEFAULT-FIVE DOF-INPUT-SIX TYPE-L
13 49
TIMEFUNCTION 1 IFLIB-2 FPAR1-2.203E06 FPAR2-0
LOADS CONCENTRATED TYPE-NODES
    138 3 3250 1 0
*
FRAME
VIEW ID-1 XVIEW-1 YVIEW-0 ZVIEW-0 ROTATION-0
VIEW ID-2 XVIEW-1 YVIEW-1 ZVIEW-1 ROTATION-0
DEPICTION SHELL-TOPBOTTOM
MESH V-1 NODES-30 ELEMENT-1 BCODE-ALL HIDDEN-DASHED
FRAME
MESH V-2 NODES-30 ELEMENT-1 BCODE-ALL HIDDEN-DASHED
*
ADINA
*
END
```

ADINA-IN VERSION 3.0.3. 22 FEBRUARY 1993
Mild Steel 12.5mm AT 60 DEG. - LOAD 1

ADINA ORIGINAL
0.03670

XVMIN -0.1651
XVMAX 0.3120
YVMIN -0.2735
YVMAX 0.01270

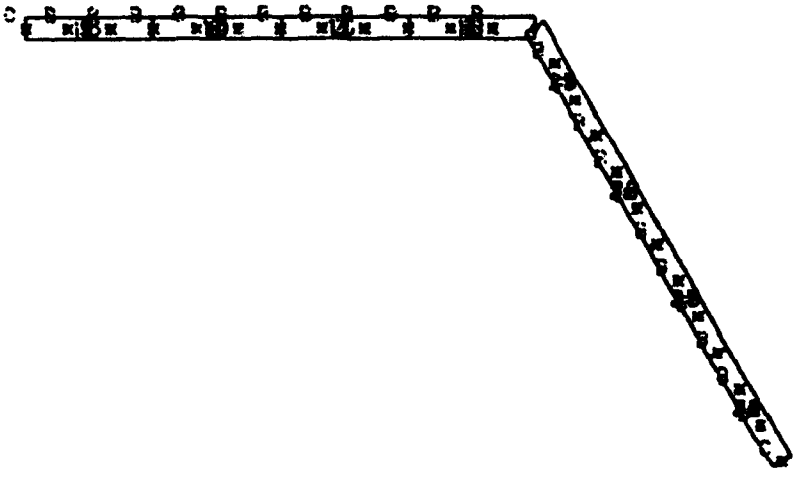

U1 U2 U3 θ1 θ2 θ3
B / / / / / -
C - - - - - -

ADINA-IN VERSION 3.0.3. 22 FEBRUARY 1993
Mild Steel 12.5mm AT 60 DEG. - LOAD 1

ADINA ORIGINAL
0.04310

XVMIN -0.2282
XVMAX 0.3321
YVMIN -0.4100
YVMAX 0.1371

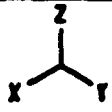

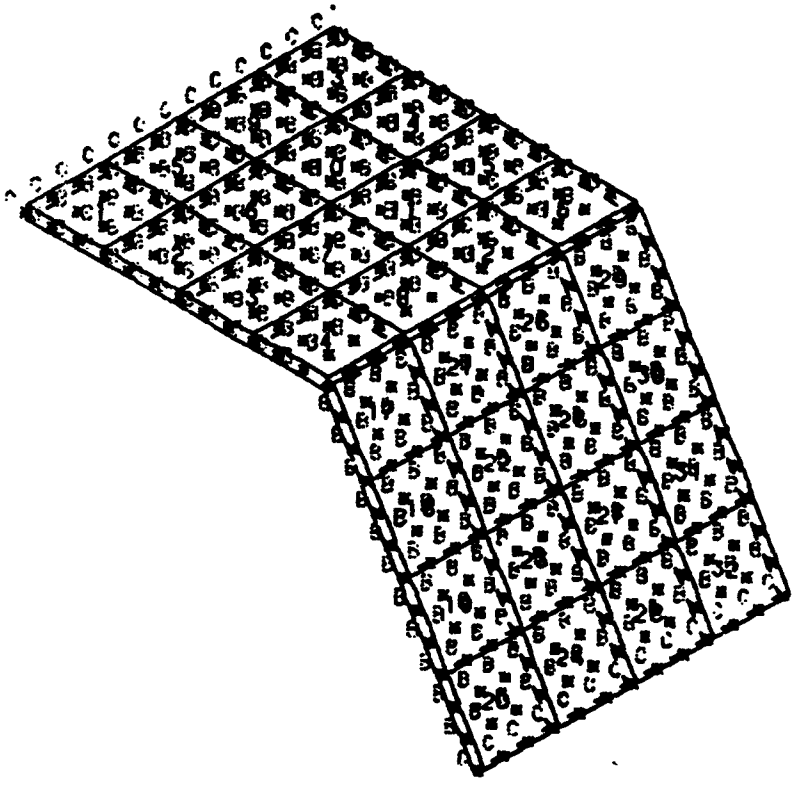

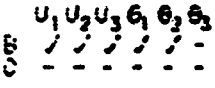

```
*     A D I N A - P L O T   4 . 0   I N P U T   F I L E
*
*            60 DEGREE PLATE
*
FILEUNITS LIST=8 LOG=7 ECHO=7
FCONTROL HEADING=UPPER ORIGIN=LOWERLEFT
CONTROL PLOTUNIT=PERCENT HEIGHT=1.25
WORKSTATION SYSTEM=13 BACKGROUND=WHITE
*
* DATABASE COMMANDS TO LOAD OR OPEN THE ADINA-PLOT DATABASE
*
DATABASE CREATE FORMATTED=YES
*DATABASE OPEN
*
*
RESPONSETYPE LOAD_STEP
NPOINT CENTER NODE=265
*
FRAME
GRAPH TIME NULL X-ACCELERATION CENTER SYMB=1 OUTPUT=ALL SUBFRAME=1133
GRAPH TIME NULL Y-ACCELERATION CENTER SYMB=1 OUTPUT=ALL SUBFRAME=1132
GRAPH TIME NULL Z-ACCELERATION CENTER SYMB=1 OUTPUT=ALL SUBFRAME=1131
ALIAS AX X-ACCELERATION
ALIAS AY Y-ACCELERATION
ALIAS AZ Z-ACCELERATION
RESULTANT ACC 'SQRT(AX**2 + AY**2 + AZ**2)'
FRAME
GRAPH TIME NULL ACC CENTER SYMB=1 OUTPUT=ALL
*
RESULTANT WYE '-(0.5*AY - 0.866*AZ)'
RESULTANT ZEE '-(0.866*AY + 0.5*AZ)'
RESULTANT ACCC 'SQRT(WYE**2 + ZEE**2 + AX**2)'
FRAME
GRAPH TIME NULL ZEE CENTER SYMB=1 OUTPUT=ALL
FRAME
GRAPH TIME NULL ACCC CENTER SYMB=1 OUTPUT=ALL
*
PMAX CENTER NUMBER=1 VAR=ACC
*
*
* CHECK LISTING
*
CONTROL EJECT=NO LINPAG=10000
FILEUNITS LIST=9
PLIST CENTER VAR=ACCC
PLIST CENTER VAR=ZEE
PLIST CENTER VAR=ACC
*
END
```

ADINA-PLOT VERSION 4.0.3. 22 FEBRUARY 1993
Mild Steel 12.5mm AT 60 DEG. - LOAD 1

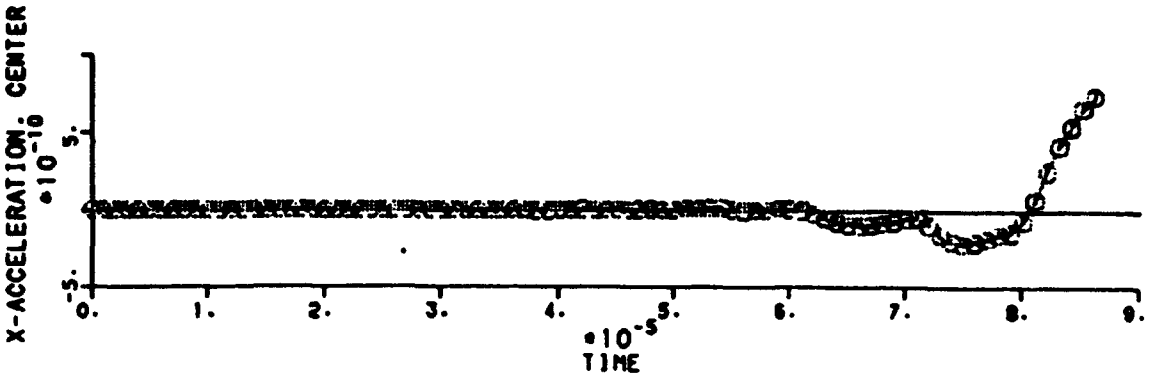

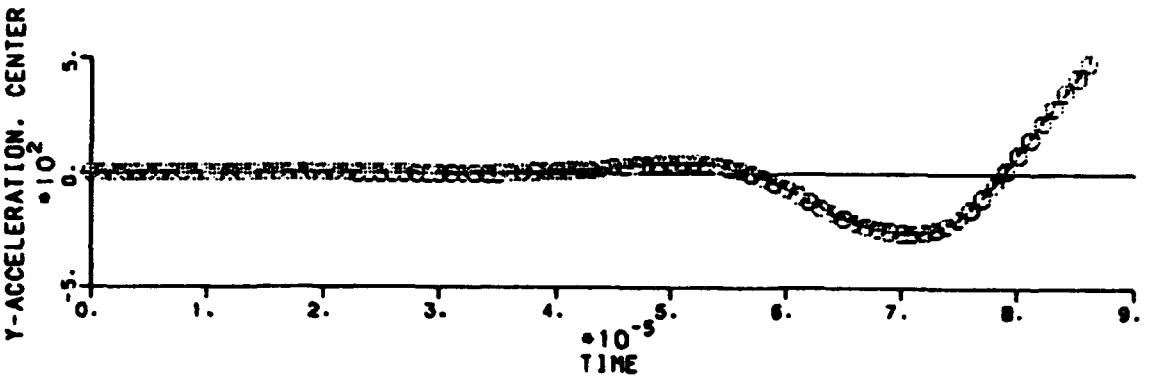

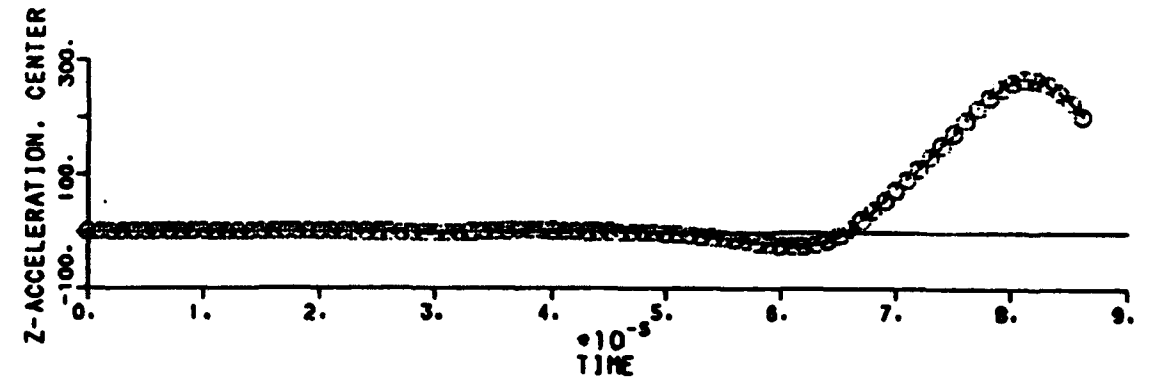

ADINA-PLOT VERSION 4.0.3, 22 FEBRUARY 1993
Mild Steel 12.5mm AT 60 DEG. - LOAD 1

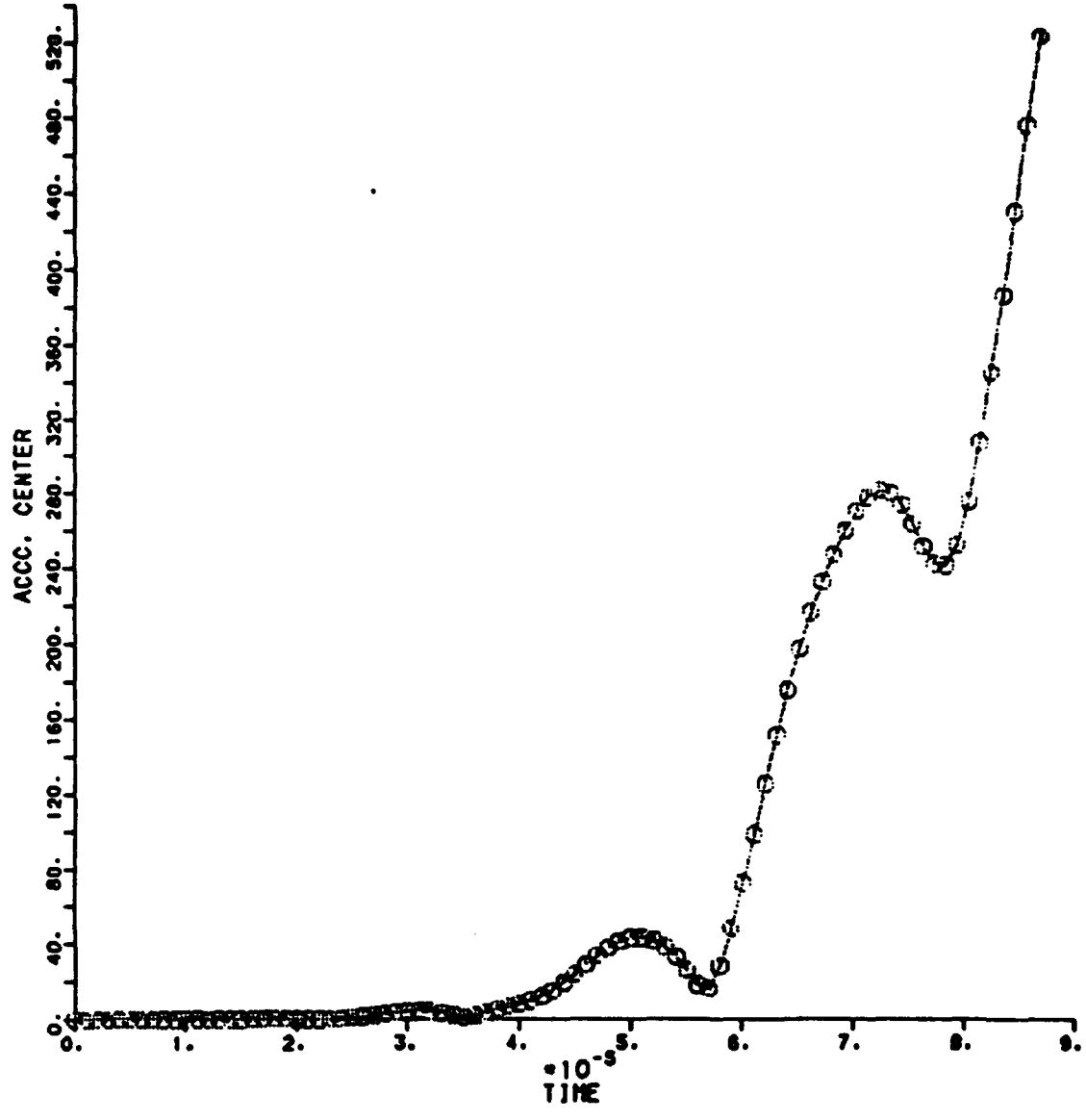

ADINA-PLOT VERSION 4.0.3, 22 FEBRUARY 1993: Mild Steel 12.5mm AT 60 DEG. - LOAD
FOR USE BY U.S. Army Ballistic Research Lab (Aberdeen Prov. Grn, LICENSED FROM
FINITE ELEMENT PROGRAM ADINA : RESPONSE TYPE LOAD_STEP
LISTING FOR POINT CENTER

TIME	ACCC
0.00000E+00	0.00000E+00
1.00000E-06	9.30238E-04
2.00000E-06	4.20475E-03
3.00000E-06	9.30784E-03
4.00000E-06	1.44745E-02
5.00000E-06	1.90816E-02
6.00000E-06	2.43270E-02
7.00000E-06	3.23849E-02
8.00000E-06	4.41949E-02
9.00000E-06	5.70080E-02
1.00000E-05	6.32841E-02
1.10000E-05	5.21622E-02
1.20000E-05	1.37955E-02
1.30000E-05	5.70139E-02
1.40000E-05	1.52565E-01
1.50000E-05	2.56309E-01
1.60000E-05	3.43909E-01
1.70000E-05	3.91448E-01
1.80000E-05	3.83494E-01
1.90000E-05	3.17996E-01
2.00000E-05	2.05074E-01
2.10000E-05	6.18036E-02
2.20000E-05	1.23525E-01
2.30000E-05	3.38790E-01
2.40000E-05	6.29607E-01
2.50000E-05	1.03897E+00
2.60000E-05	1.60110E+00
2.70000E-05	2.31449E+00
2.80000E-05	3.12007E+00
2.90000E-05	3.89485E+00
3.00000E-05	4.46799E+00
3.10000E-05	4.65949E+00
3.20000E-05	4.33322E+00
3.30000E-05	3.45249E+00
3.40000E-05	2.14884E+00
3.50000E-05	1.16318E+00
3.60000E-05	2.21459E+00
3.70000E-05	3.85465E+00
3.80000E-05	5.36075E+00
3.90000E-05	6.70279E+00
4.00000E-05	8.07655E+00
4.10000E-05	9.78638E+00
4.20000E-05	1.21172E+01
4.30000E-05	1.52434E+01
4.40000E-05	1.91905E+01
4.50000E-05	2.38127E+01
4.60000E-05	2.87883E+01
4.70000E-05	3.36609E+01
4.80000E-05	3.79260E+01
4.90000E-05	4.11288E+01
5.00000E-05	4.29321E+01
5.10000E-05	4.31298E+01
5.20000E-05	4.16056E+01
5.30000E-05	3.82675E+01
5.40000E-05	3.30197E+01
5.50000E-05	2.59109E+01
5.60000E-05	1.81054E+01

5.70000E-05	1.63657E+01
5.80000E-05	2.83464E+01
5.90000E-05	4.81993E+01
6.00000E-05	7.21315E+01
6.10000E-05	9.83565E+01
6.20000E-05	1.25315E+02
6.30000E-05	1.51541E+02
6.40000E-05	1.75864E+02
6.50000E-05	1.97590E+02
6.60000E-05	2.16566E+02
6.70000E-05	2.33043E+02
6.80000E-05	2.47402E+02
6.90000E-05	2.59835E+02
7.00000E-05	2.70118E+02
7.10000E-05	2.77564E+02
7.20000E-05	2.81178E+02
7.30000E-05	2.80033E+02
7.40000E-05	2.73791E+02
7.50000E-05	2.63335E+02
7.60000E-05	2.51321E+02
7.70000E-05	2.42256E+02
7.80000E-05	2.41429E+02
7.90000E-05	2.52466E+02
8.00000E-05	2.75357E+02
8.10000E-05	3.07242E+02
8.20000E-05	3.44820E+02
8.30000E-05	3.85903E+02
8.40000E-05	4.29564E+02
8.50000E-05	4.75520E+02
8.60000E-05	5.23346E+02

ADINA-PLOT VERSION 4.0.3, 22 FEBRUARY 1993: Mild Steel 12.5mm AT 60 DEG. - LOAD
FOR USE BY U.S. Army Ballistic Research Lab (Aberdeen Prov. Grn, LICENSED FROM
FINITE ELEMENT PROGRAM ADINA : RESPONSE TYPE LOAD_STEP
LISTING FOR POINT CENTER

TIME	ZEE
0.00000E+00	0.00000E+00
1.00000E-06	9.30238E-04
2.00000E-06	4.20475E-03
3.00000E-06	9.30783E-03
4.00000E-06	1.44745E-02
5.00000E-06	1.90815E-02
6.00000E-06	2.43267E-02
7.00000E-06	3.23840E-02
8.00000E-06	4.41917E-02
9.00000E-06	5.69998E-02
1.00000E-05	6.32650E-02
1.10000E-05	5.21124E-02
1.20000E-05	1.34217E-02
1.30000E-05	-5.68410E-02
1.40000E-05	-1.52436E-01
1.50000E-05	-2.56150E-01
1.60000E-05	-3.43674E-01
1.70000E-05	-3.91068E-01
1.80000E-05	-3.82860E-01
1.90000E-05	-3.16917E-01
2.00000E-05	-2.03085E-01
2.10000E-05	-5.51267E-02
2.20000E-05	1.21199E-01
2.30000E-05	3.38382E-01
2.40000E-05	6.29550E-01
2.50000E-05	1.03896E+00
2.60000E-05	1.60104E+00

2.70000E-05	2.31400E+00
2.80000E-05	3.11780E+00
2.90000E-05	3.88760E+00
3.00000E-05	4.44953E+00
3.10000E-05	4.61885E+00
3.20000E-05	4.25139E+00
3.30000E-05	3.29252E+00
3.40000E-05	1.80530E+00
3.50000E-05	-3.56162E-02
3.60000E-05	-1.98795E+00
3.70000E-05	-3.81391E+00
3.80000E-05	-5.35935E+00
3.90000E-05	-6.61365E+00
4.00000E-05	-7.72718E+00
4.10000E-05	-8.97560E+00
4.20000E-05	-1.06774E+01
4.30000E-05	-1.30875E+01
4.40000E-05	-1.63003E+01
4.50000E-05	-2.01939E+01
4.60000E-05	-2.44356E+01
4.70000E-05	-2.85479E+01
4.80000E-05	-3.20132E+01
4.90000E-05	-3.43809E+01
5.00000E-05	-3.53382E+01
5.10000E-05	-3.47187E+01
5.20000E-05	-3.24466E+01
5.30000E-05	-2.84398E+01
5.40000E-05	-2.25151E+01
5.50000E-05	-1.43438E+01
5.60000E-05	-3.48947E+00
5.70000E-05	1.04645E+01
5.80000E-05	2.77307E+01
5.90000E-05	4.81333E+01
6.00000E-05	7.09919E+01
6.10000E-05	9.51288E+01
6.20000E-05	1.19018E+02
6.30000E-05	1.41051E+02
6.40000E-05	1.59839E+02
6.50000E-05	1.74477E+02
6.60000E-05	1.84662E+02
6.70000E-05	1.90624E+02
6.80000E-05	1.92888E+02
6.90000E-05	1.91923E+02
7.00000E-05	1.87792E+02
7.10000E-05	1.79937E+02
7.20000E-05	1.67168E+02
7.30000E-05	1.47905E+02
7.40000E-05	1.20593E+02
7.50000E-05	8.42003E+01
7.60000E-05	3.86263E+01
7.70000E-05	-1.51032E+01
7.80000E-05	-7.49329E+01
7.90000E-05	-1.38151E+02
8.00000E-05	-2.01933E+02
8.10000E-05	-2.63901E+02
8.20000E-05	-3.22513E+02
8.30000E-05	-3.77168E+02
8.40000E-05	-4.27992E+02
8.50000E-05	-4.75364E+02
8.60000E-05	-5.19355E+02

ADINA-PLOT VERSION 4.0.3, 22 FEBRUARY 1993: Mild Steel 12.5mm AT 60 DEG. - LOAD FOR USE BY U.S. Army Ballistic Research Lab (Aberdeen Prov. Grn, LICENSED FROM FINITE ELEMENT PROGRAM ADINA : RESPONSE TYPE LOAD_STEP

APPENDIX B:

TABULATED EXPERIMENTAL DATA

INTENTIONALLY LEFT BLANK.

This appendix contains the tabulated experimental data. The tables that follow present the defining acceleration for each experiment conducted as part of this effort as well as mean values and standard deviations.

MILD STEEL PLATES:

Angle (Radians)	Load No.	Acc. (M/S^2)	Mean	Std. Dev.
0.00	1	146.3		
0.00	1	183.0		
0.00	1	192.9	173.5	27.5
0.00	1	202.7		
0.00	1	142.4		
0.00	2	485.5		
0.00	2	285.8		
0.00	2	438.1	412.6	62.3
0.00	2	343.1		
0.00	2	383.7		
0.00	3	657.6		
0.00	3	610.1		
0.00	3	626.9	640.9	69.4
0.00	3	561.6		
0.00	3	748.5		
0.26	1	159.6		
0.26	1	162.2		
0.26	1	134.5	159.1	14.4
0.26	1	169.1		
0.26	1	170.0		
0.26	2	413.4		
0.26	2	403.5		
0.26	2	355.0	404.2	31.9
0.26	2	405.4		
0.26	2	443.9		
1.31	1	139.5		
1.31	1	112.7		
1.31	1	134.5	127.2	10.6
1.31	1	121.6		
1.31	1	127.6		
1.31	2	275.9		
1.31	2	228.4		
1.31	2	282.8	279.4	33.4
1.31	2	288.7		
1.31	2	321.3		
1.31	3	540.9		
1.31	3	413.4		
1.31	3	413.4	468.5	64.7
1.31	3	439.0		
1.31	3	536.0		
1.57	1	179.2		
1 57	1	183.0		
1.57	1	152.0	159.9	27.6
1.57	1	108.9		
1.57	1	160.7		
1.57	1	175.5		

MILD STEEL PLATES:

Angle (Radians)	Load No.	Acc. (M/S^2)	Mean	Std. Dev.
1.57	2	292.9		
1.57	2	300.4		
1.57	2	278.1	301.3	18.3
1.57	2	327.5		
1.57	2	307.8		
1.57	3	349.8		
1.57	3	426.4		
1.57	3	390.6	420.7	68.7
1.57	3	541.4		
1.57	3	370.8		
1.57	3	445.0		
2.09	1	185.4		
2.09	1	126.1		
2.09	1	125.6	157.4	33.5
2.09	1	198.3		
2.09	1	151.8		
2.09	2	312.4		
2.09	2	284.3		
2.09	2	330.8	348.7	56.9
2.09	2	415.3		
2.09	2	400.9		
2.09	3	677.4		
2.09	3	641.7		
2.09	3	703.1	691.7	28.5
2.09	3	713.9		
2.09	3	718.8		
2.09	3	695.1		

ALUMINUM PLATES:

Angle (Radians)	Load No.	Acc. (M/S^2)	Mean	Std. Dev.
0.00	1	185.4		
0.00	1	188.2		
0.00	1	198.7	193.4	6.1
0.00	1	197.3		
0.00	1	197.3		
0.00	2	352.8		
0.00	2	397.8		
0.00	2	389.1	375.5	19.1
0.00	2	359.7		
0.00	2	378.2		
0.00	3	585.3		
0.00	3	595.2		
0.00	3	613.7	561.2	73.4
0.00	3	432.0		
0.00	3	579.7		
0.52	1	137.2		
0.52	1	140.5		

ALUMINUM PLATES:

Angle (Radians)	Load No.	Acc. (M/S^2)	Mean	Std. Dev.
0.52	1	142.0	143.6	5.5
0.52	1	150.9		
0.52	1	147.6		
0.52	2	275.9		
0.52	2	254.4		
0.52	2	287.3	273.6	12.2
0.52	2	278.8		
0.52	2	271.8		
0.52	3	312.1		
0.52	3	308.4		
0.52	3	398.7	355.2	53.7
0.52	3	399.8		
0.52	3	9		
0.52	3	.1		
1.05	1	116.4		
1.05	1	154.6		
1.05	1	102.0	131.2	19.0
1.05	1	134.7		
1.05	1	143.5		
1.05	1	135.7		
1.05	2	277.7		
1.05	2	241.0		
1.05	2	265.5	266.8	14.8
1.05	2	269.2		
1.05	2	284.0		
1.05	2	263.2		
1.05	3	416.0		
1.05	3	360.1		
1.05	3	418.3	401.1	30.5
1.05	3	422.7		
1.05	3	426.1		
1.05	3	364.2		
1.57	1	203.9		
1.57	1	203.9		
1.57	1	178.0	191.1	13.0
1.57	1	178.0		
1.57	1	191.6		
1.57	2	403.0		
1.57	2	427.7		
1.57	2	360.9	391.2	30.0
1.57	2	373.3		
1.57	3	582.1		
1.57	3	620.4	585.5	37.8
1.57	3	534.0		
1.57	3	605.6		
2.09	1	142.1		
2.09	1	164.1		
2.09	1	158.2	156.2	9.0
2.09	1	153.3		
2.09	1	163.2		
2.09	2	273.2		
2.09	2	294.2		
2.09	2	179.2	257.6	47.9

ALUMINUM PLATES:

Angle (Radians)	Load No.	Acc. (M/S^2)	Mean	Std. Dev.
2.09	2	247.2		
2.09	2	294.2		
2.09	3	458.6		
2.09	3	519.1		
2.09	3	530.3	506.8	32.0
2.09	3	490.7		
2.09	3	535.2		

APPENDIX C:

FOURTH-ORDER EQUATIONS

INTENTIONALLY LEFT BLANK.

This appendix contains the fourth-order polynomial equations that were derived for the experimental data. The equations are provided to show the increased R^2 values and to allow further investigation by interested readers. The equations are as follows:

Mild Steel: Load 1: $R^2 = 0.24$

$$ACC = 166.39 + 152.06\,(ANG) - 423.69\,(ANG)^2 + 315.12\,(ANG)^3 - 70.82\,(ANG)^4$$

$$ATT = 1 + 0.914\,(ANG) - 2.55\,(ANG)^2 + 1.89\,(ANG)^3 - 0.43\,(ANG)^4$$

Mild Steel: Load 2: $R^2 = 0.56$

$$ACC = 387.36 + 274.68\,(ANG) - 951.15\,(ANG)^2 + 730.96\,(ANG)^3 - 164.13\,(ANG)^4$$

$$ATT = 1 + 0.71\,(ANG) - 2.46\,(ANG)^2 + 1.89\,(ANG)^3 - 0.42\,(ANG)^4$$

Mild Steel: Load 3: $R^2 = 0.72$

$$ACC = 661.3 + 87.59\,(ANG) - 619.47\,(ANG)^2 + 381.12\,(ANG)^3 - 48.74\,(ANG)^4$$

$$ATT = 1 + 0.132\,(ANG) - 0.94\,(ANG)^2 + 0.58\,(ANG)^3 - 0.07\,(ANG)^4$$

Aluminum: Load 1: $R^2 = 0.85$

$$ACC = 193.38 - 12.3\,(ANG) - 335.42\,(ANG)^2 + 395.61\,(ANG)^3 - 113.1\,(ANG)^4$$

$$ATT = 1 - 0.064\,(ANG) - 1.73\,(ANG)^2 + 2.05\,(ANG)^3 - 0.58\,(ANG)^4$$

Aluminum: Load 2: $R^2 = 0.84$

$$ACC = 375.52 - 58.85\,(ANG) - 610.82\,(ANG)^2 + 791.91\,(ANG)^3 - 238.8\,(ANG)^4$$

$$ATT = 1 - 0.157\,(ANG) - 1.63\,(ANG)^2 + 2.12\,(ANG)^3 - 0.636\,(ANG)^4$$

Aluminum: Load 3: $R^2 = 0.81$

$$ACC = 561.18 - 566.87\,(ANG) + 173.79\,(ANG)^2 + 381.93\,(ANG)^3 - 163.29\,(ANG)^4$$

$$ATT = 1 - 1.01\,(ANG) + 0.31\,(ANG)^2 + 0.68\,(ANG)^3 - 0.29\,(ANG)^4$$

No. of Copies	Organization
2	Administrator Defense Technical Info Center ATTN: DTIC-DDA Cameron Station Alexandria, VA 22304-6145
1	Commander U.S. Army Materiel Command ATTN: AMCAM 5001 Eisenhower Ave. Alexandria, VA 22333-0001
1	Director U.S. Army Research Laboratory ATTN: AMSRL-OP-CI-AD, Tech Publishing 2800 Powder Mill Rd. Adelphi, MD 20783-1145
1	Director U.S. Army Research Laboratory ATTN: AMSRL-OP-CI-AD, Records Management 2800 Powder Mill Rd. Adelphi, MD 20783-1145
2	Commander U.S. Army Armament Research, Development, and Engineering Center ATTN: SMCAR-TDC Picatinny Arsenal, NJ 07806-5000
1	Director Benet Weapons Laboratory U.S. Army Armament Research, Development, and Engineering Center ATTN: SMCAR-CCB-TL Watervliet, NY 12189-4050
1	Director U.S. Army Advanced Systems Research and Analysis Office (ATCOM) ATTN: AMSAT-R-NR, M/S 219-1 Ames Research Center Moffett Field, CA 94035-1000

No. of Copies	Organization
1	Commander U.S. Army Missile Command ATTN: AMSMI-RD-CS-R (DOC) Redstone Arsenal, AL 35898-5010
1	Commander U.S. Army Tank-Automotive Command ATTN: AMSTA-JSK (Armor Eng. Br.) Warren, MI 48397-5000
1	Director U.S. Army TRADOC Analysis Command ATTN: ATRC-WSR White Sands Missile Range, NM 88002-5502
(Class. only) 1	Commandant U.S. Army Infantry School ATTN: ATSH-CD (Security Mgr.) Fort Benning, GA 31905-5660
(Unclass. only) 1	Commandant U.S. Army Infantry School ATTN: ATSH-WCB-O Fort Benning, GA 31905-5000
1	WL/MNOI Eglin AFB, FL 32542-5000
	Aberdeen Proving Ground
2	Dir, USAMSAA ATTN: AMXSY-D AMXSY-MP, H. Cohen
1	Cdr, USATECOM ATTN: AMSTE-TC
1	Dir, USAERDEC ATTN: SCBRD-RT
1	Cdr, USACBDCOM ATTN: AMSCB-CII
1	Dir, USARL ATTN: AMSRL-SL-I
5	Dir, USARL ATTN: AMSRL-OP-AP-L

No. of Copies	Organization
19	Dir, USARL ATTN: AMSRL-WT-TB, F. Gregory J. Santiago N. Gniazdowski AMSRL-CI-S, B. Bodt AMSRL-SL-BS, R. Grote (5) (328) J. Jacobson (328) R. Kirby (328) D. Petty (328) M. Sivack (328) W. Robinson (1190) E. Quigley (TR#3) AMSRL-SL-BA, J. Walbert (1065) AMSRL-SL-BG, J. Liu (328) AMSRL-SL-B, P. Deitz (328) J. Morrisey (328)
1	Dir, USACSTA ATTN: STECS-OA-I, S. Walton

This Laboratory undertakes a continuing effort to improve the quality of the reports it publishes. Your comments/answers to the items/questions below will aid us in our efforts.

1. ARL Report Number ARL-TR-466 Date of Report June 1994

2. Date Report Received _____

3. Does this report satisfy a need? (Comment on purpose, related project, or other area of interest for which the report will be used.) _____

4. Specifically, how is the report being used? (Information source, design data, procedure, source of ideas, etc.) _____

5. Has the information in this report led to any quantitative savings as far as man-hours or dollars saved, operating costs avoided, or efficiencies achieved, etc? If so, please elaborate. _____

6. General Comments. What do you think should be changed to improve future reports? (Indicate changes to organization, technical content, format, etc.) _____

CURRENT ADDRESS

_____
Organization

_____
Name

_____
Street or P.O. Box No.

_____
City, State, Zip Code

7. If indicating a Change of Address or Address Correction, please provide the Current or Correct address above and the Old or Incorrect address below.

OLD ADDRESS

_____
Organization

_____
Name

_____
Street or P.O. Box No.

_____
City, State, Zip Code

(Remove this sheet, fold as indicated, tape closed, and mail.)
(DO NOT STAPLE)

DEPARTMENT OF THE ARMY

OFFICIAL BUSINESS

BUSINESS REPLY MAIL
FIRST CLASS PERMIT No 0001, APG, MD

Postage will be paid by addressee.

Director
U.S. Army Research Laboratory
ATTN: AMSRL-OP-CI-B (Tech Lib)
Aberdeen Proving Ground, MD 21005-5066

NO POSTAGE
NECESSARY
IF MAILED
IN THE
UNITED STATE